WHIM Syndrome-linked CXCR4 mutations drive osteoporosis

Adrienne Anginot, Julie Nguyen, Zeina Abou Nader, Vincent Rondeau, Amélie Bonaud, Maria Kalogeraki, Antoine Boutin, Julia Lemos, Valeria Bisio, Joyce Koenen, et al.

Using a mouse model harboring a WHIM Syndrome-linked gain-of-function CXCR4 mutation and bone marrow samples from WHIM patients, the authors show that proper CXCR4 signaling termination is essential for bone tissue homeostasis.

WHIM Syndrome-linked *CXCR4* mutations drive osteoporosis

Adrienne Anginot[1,2,3,#], Julie Nguyen[2,4,#], Zeina Abou Nader[1,2,3,#], Vincent Rondeau[1,2,3], Amélie Bonaud[1,2,3], Maria Kalogeraki[1,2,3], Antoine Boutin[5], Julia Lemos[1,2,3], Valeria Bisio[1,2,3], Joyce Koenen[2,4], Léa Sakr[6], Amandine Picart[6], Amélie Coudert[6], Sylvain Provot[6], Nicolas Dulphy[1,2,3], Michel Aurrand-Lions[2,7], Stéphane J.C. Mancini[2,7], Gwendal Lazennec[2,8], David H. McDermott[9], Fabien Guidez[3,10], Claudine Blin-Wakkach[5], Philip M. Murphy[9], Martine Cohen-Solal[6], Marion Espéli[1,2,3,£], Matthieu Rouleau[5,£], and Karl Balabanian[1,2,3,*]

[1]Université Paris Cité, Institut de Recherche Saint-Louis, INSERM U1160, Paris, France.
[2]CNRS, GDR3697 "Microenvironment of tumor niches", Micronit, France.
[3]OPALE Carnot Institute, The Organization for Partnerships in Leukemia, Hôpital Saint-Louis, Paris, France.
[4]Inflammation, Chemokines and Immunopathology, INSERM, Université Paris-Saclay, Clamart, France.
[5]Université Côte d'Azur, CNRS, LP2M, Nice, France.
[6]Université Paris Cité, BIOSCAR Inserm U1132, Department of Rheumatology and Reference Center for Rare Bone Diseases, AP-HP Hospital Lariboisière, Paris, France.
[7]Aix Marseille Univ, CNRS, INSERM, Institut Paoli-Calmettes, CRCM, Marseille, France.
[8]CNRS, SYS2DIAG-ALCEDIAG, Cap Delta, Montpellier, France.
[9]Molecular Signaling Section, Laboratory of Molecular Immunology, National Institute of Allergy and Infectious Diseases, NIH, Bethesda, MD.
[10]Université Paris Cité, Institut de Recherche Saint-Louis, INSERM U1131, Paris, France.
[#]AA, JN and ZA-N: these authors contributed equally.
[£]ME and MR: these authors contributed equally.
*Correspondence & lead contact: karl.balabanian@inserm.fr.

Abbreviations: BMSC: Bone marrow stromal cell; C-tail: Carboxyl-terminal tail; HSPC: Hematopoietic stem and progenitor cell; MFI: Mean fluorescence intensity; OBL: Osteoblast; OCL: Osteoclast; Ocn: Osteocalcin; OPC: Osteoblastic progenitor; Opn: Osteopontin; Osx: Osterix; SLAM: Signaling lymphocyte activation molecule; SSC: Skeletal stromal/stem cell; WS: Warts, Hypogammaglobulinemia, Infections and Myelokathexis Syndrome.

ABSTRACT

WHIM Syndrome is a rare immunodeficiency caused by gain-of-function *CXCR4* mutations. Here we report a decrease in bone mineral density in 25% of WHIM patients and bone defects leading to osteoporosis in a WHIM mouse model. Imbalanced bone tissue is observed in mutant mice combining reduced osteoprogenitor cells and increased osteoclast numbers. Mechanistically, impaired CXCR4 desensitization disrupts cell cycle progression and osteogenic commitment of skeletal stromal/stem cells, while increasing their pro-osteoclastogenic capacities. Impaired osteogenic differentiation is evidenced in primary bone marrow stromal cells from WHIM patients. In mice, chronic treatment with the CXCR4 antagonist AMD3100 normalizes *in vitro* osteogenic fate of mutant skeletal stromal/stem cells and reverses *in vivo* the loss of skeletal cells, demonstrating that proper CXCR4 desensitization is required for the osteogenic specification of skeletal stromal/stem cells. Our study provides mechanistic insights into how CXCR4 signaling regulates the osteogenic fate of skeletal cells and the balance between bone formation and resorption.

Keywords: Skeletal stromal/stem cell; Bone marrow; CXCR4 signaling; Osteogenesis; WHIM Syndrome; Osteoporosis.

INTRODUCTION

The bone marrow (BM) is a complex structural and primary immune organ whose development and maintenance depend on multiple cell types including cells of the hematopoietic lineage like hematopoietic stem and progenitor cells (HSPCs), but also vascular cells and numerous skeletal cells encompassing BM stromal cells (BMSCs), skeletal progenitor/precursor cells as well as bone-making osteoblasts (OBLs)[1,2]. Together these cells compose specialized micro-anatomical structures called "niches" that sustain their survival and differentiation[3-9]. For instance, the HSPC niches are thought to be composed of perivascular stromal units associated with sinusoids and arterioles[10-15]. Bone and adipose cells are thought to derive from subsets of BMSCs that are located near blood vessels and function as skeletal stromal/stem cells (SSCs)[16-19]. However, the exact localization, composition and crossover of these niches in relation with bone function are not yet established. Bone tissue homeostasis relies on the balance between formation and resorption of bone matrix mediated by effector cells that derive from SSCs and HSPCs respectively. Disequilibrium of this balance can lead to diseases such as osteoporosis or osteopetrosis. In such a landscape, SSCs are key players: not only they give rise to OBLs but they also contribute to perivascular structures important for HSPCs[20-28]. Understanding how SSCs maintain their identity, achieve plasticity and support hematopoiesis in adult BM is thus an important emerging field[3,6,9,12,29]. Recently, Ambrosi and coll. showed that intrinsic ageing of SSCs skews skeletal and hematopoietic lineage outputs, leading to fragile bones[30]. Moreover, Jeffery and coll. reported how BM and periosteal SSCs contribute to bone maintenance and repair[31]. However, both extrinsic and intrinsic mechanisms regulating their fate remain incompletely understood.

In adult BM, signaling by the G protein-coupled receptor CXCR4 on HSPCs in response to stimulation by the chemokine CXCL12/Stromal cell-derived factor-1, produced by BMSCs constitutes a key pathway through which the stromal niches and HSPCs communicate[32-37].

Conditional ablation of *Cxcl12* from perivascular stromal cells or OBLs demonstrated that HSCs occupy a perivascular but not an endosteal niche[21,38], whereas targeted deletion of *Cxcl12* from BM stromal cells has allowed the identification of specialized niches supporting leukemia stem cell maintenance[39]. Both Cxcr4 and Cxcl12 are broadly expressed by non-hematopoietic tissues and cell types and have multifunctional roles beyond hematopoiesis. Since mice deficient for *Cxcr4* or *Cxcl12* die perinatally, our understanding of the role of the Cxcl12/Cxcr4 axis in regulating the BM ecosystem is mostly based on relatively selective loss-of-function models[21,40-44]. Conditional inactivation of *Cxcl12* or *Cxcr4* in paired-related homeobox gene 1 (Prx1)- or osterix (Osx)-expressing cells, *i.e.* respectively multipotent mesenchymal progenitors or osteoprogenitor cells (OPCs) and descendant OBLs, was associated with reduced postnatal bone formation, suggesting a positive regulatory role of this pair in OBL development and/or function[21,43,44]. Single cell transcriptomics recently suggested heterogeneity within adult Cxcl12- or Leptin-receptor (LepR)-expressing mesenchymal cells poised to undergo either adipogenic or osteogenic specification[45,46]. However, it is still unclear whether and how Cxcr4 signaling regulates intrinsically osteogenic specification of skeletal cells.

Here, we addressed this point using as a paradigm the WHIM Syndrome (WS), a rare immunodeficiency caused by viable inherited heterozygous gain-of-function mutations in *CXCR4* affecting homologous desensitization of the receptor, thus resulting in enhanced signaling following CXCL12 stimulation, defective lymphoid differentiation of HSPCs and reduced blood leukocyte numbers[47-50]. Taking advantage of a mouse strain that harbors the naturally occurring WS-linked heterozygous $CXCR4^{S338X}$ mutation ($Cxcr4^{+/1013}$, +/1013)[51-54], and of human BM samples from WS donors and clinical data from 19 WS patients, we investigated whether WS mutations affect the SSC landscape with a particular attention given to the bone fraction. WS-linked *CXCR4* mutations were associated with reduced bone mass in mice and humans. In mice, this relied on impaired CXCR4 desensitization that disrupts cell

cycle progression and osteogenic commitment of SSCs, while paradoxically increasing the pro-osteoclastogenic capacities of these cells. Impairment in osteogenic potential was also evidenced in BMSCs from WS patients. Thus, proper CXCR4 desensitization is required for the osteogenic specification of bone SSCs.

RESULTS

WS-linked *CXCR4* mutations are associated with reduced bone mass in mice and humans

Following CXCL12 stimulation, β-arrestins are recruited to the carboxyl-terminal tail (C-tail) domain of CXCR4, precluding further G-protein activation (*i.e.* desensitization) and leading to receptor internalization[55]. Both processes are dysregulated in WS most often due to autosomal-dominant gain-of-function mutations that result in the distal truncation of the C-tail of CXCR4 and a desensitization-resistant, hyperactive receptor[56]. Although the impact of these WS mutations on immune cells is currently being understood[51-54,57], nothing is known about their impact on the skeletal landscape. Bone mineral density (BMD) values were measured in 19 patients with WS for lumbar spine and femoral neck by total body dual-energy X-ray absorptiometry. BMD T- and Z-scores were found to be low at least in one site in five patients (Table 1). Likewise, this was evidenced in adult (8-12-week-old) *Cxcr4*^{1013}-bearing (*i.e.* heterozygous [+/1013] and homozygous [1013/1013]) mice, as compared to *Cxcr4*$^{+/+}$ (WT) mice. Analyses of lumbar spine revealed decreased BMD values in mutant mice, in a *Cxcr4*^{1013} allele dose-dependent manner (Fig. 1A). Micro-computed tomography (μCT) analyses further unraveled a reduction in trabecular and cortical bone in mutant mice (Fig. 1B). In mutant femurs, there was a reduction in the trabecular bone density that followed a *Cxcr4*^{1013} allele copy number-dependent pattern. This was characterized by a significant decrease in bone volume and trabecular numbers, while the trabecular separation was increased compared to WT mice (Fig. 1C). The cortical bone volume and thickness were also affected (Fig. 1B and 1D). This gene-dependent reduction was observed among both female and male mutant mice. Histomorphometric analyses confirmed decreased bone volume and trabecular numbers in mutant mice as shown by toluidine blue and osteopontin (Opn) staining (Fig. 1E and 1F). Strikingly, staining for Alcian Blue and perilipin that are used for chondrocyte and adipocyte identification respectively, were unaltered in mutant bone (Fig. 1G and 1H). Consistently, the

thickness of the growth plate as well as the adipocyte content were similar in mice carrying the *Cxcr4* mutation compared to WT ones (Fig. 1I and 1J), thus suggesting that Cxcr4 specifically regulates the osteogenic fate in adults. Moreover, adult mutant mice did not exhibit significant changes of body size or weight (Fig. 1K), indicating that the *Cxcr4* mutation likely does not alter the skeletal growth. Overall, these findings revealed an osteopenic skeleton in *Cxcr4*^{1013}-bearing mice and low BMD in 25% of WS patients.

Reduction of skeletal stromal cells in *Cxcr4*^{1013}-bearing mice

We then evaluated by flow cytometry the bone composition of WT and mutant mice with a focus on skeletal cells that encompass notably SSCs, OPCs and OBLs[58]. Long bones were flushed and then digested. Total stromal cells in the bone fraction were identified as negative for CD45, Lineage (including Ter119), c-Kit and CD71 expression as previously reported[12,59]. Endothelial cells were excluded based on CD31 expression. Two distinct CD51^{+} stromal cell subsets were identified based on Sca-1 and PDGFRα: SSCs (Sca-1^{+}PDGFRα^{+}) and more differentiated OPCs (Sca-1^{-}PDGFRα$^{+/-}$) (Fig. 2A). We consider Sca-1^{+}PDGFRα^{+} cells at the top of the hierarchy based on previous works that indicated a highest CFU-F clonogenic potential of these cells as compared to Sca-1^{-}PDGFRα^{+} cells[12,28,31,60]. We observed a significant decrease of the numbers of OPCs, and to a lesser extent of SSCs, that followed a *Cxcr4*^{1013} allele dose-dependent pattern (Fig. 2B), thus reinforcing that the landscape of the bone stroma is altered in *Cxcr4*^{1013}-bearing mice.

We next examined *in vitro* the function of the signaling trio formed by Cxcl12 and its two receptors Cxcr4 and Ackr3 in skeletal cells. Membrane expression of Cxcr4 and Ackr3 was similar between WT and mutant skeletal cells including SSCs (Fig. S1A and S1B). However, +/1013 and 1013/1013 SSCs displayed both impaired Cxcr4 internalization following Cxcl12 stimulation as well as increased Cxcl12-mediated chemotaxis that was abolished by the specific

158 Cxcr4 antagonist AMD3100 (Fig. S1C and S1D). These dysfunctions likely relied on the
159 enhanced signaling properties of the truncated Cxcr4 receptor as revealed by Erk PhosphoFlow
160 analyses (Fig. S1E). Combined with the apparent preserved capacity of Ackr3 to bind and
161 internalize Cxcl12 *in vitro* (Fig. S1F and S1G), these findings indicated a functional expression
162 of the desensitization-resistant C-tail-truncated $Cxcr4^{1013}$ receptor on SSCs. Abnormal Cxcr4
163 signaling was not associated with changes in apoptosis of SSCs (Fig. S1H).

164 To determine whether reduction of bone content in *Cxcr4*^{1013}-bearing mice resulted
165 from defects intrinsic to skeletal cells and/or an alteration of the hematopoietic (or another non-
166 stromal) system, we performed reciprocal long (16 weeks)- and short (3 weeks)-term BM
167 reconstitution experiments. First, BM cells from WT $CD45.1^+$ mice were transplanted into
168 lethally irradiated 8-wk old $CD45.2^+$ WT or mutant (+/1013 and 1013/1013) mice (Fig. 2C).
169 Sixteen weeks later, mutant recipients exhibited $CD45.1^+$ chimerism in hematopoietic
170 compartments similar to those of WT recipients (Fig. 2D) but displayed reduced numbers of
171 skeletal cells including SSCs and OPCs (Fig. 2E). Confocal imaging and μCT analyses
172 confirmed that transplantation of WT BM was not sufficient to rescue the trabecular network
173 in mutant recipients (Fig. 2F-I). This was also evidenced three weeks after WT BM
174 transplantation (Fig. 2G). Although we cannot formally exclude that WT hematopoietic cells
175 may be able to rescue the reduced trabecular bone content in mutant mice earlier in
176 development, these results suggested that skeletal cell-autonomous Cxcr4 regulation
177 contributes to the persistent bone defects in adult *Cxcr4*^{1013}-bearing mice. We then performed
178 reverse chimeras in which irradiated 8-wk old $CD45.1^+$ WT mice were reconstituted with WT,
179 +/1013 or 1013/1013 $CD45.2^+$ BM (Fig. 3A). Sixteen weeks later, $CD45.2^+$ chimerism of LT-
180 HSCs and leukocytes were decreased respectively in BM and blood of $CD45.1^+$ WT recipients
181 engrafted with mutant BM, confirming the impaired reconstitution capacity of mutant HSCs
182 (Fig. 3B and [49]). There were significantly lower numbers of skeletal cells and defective

trabecular bone content in *Cxcr4*^{1013}-bearing BM-chimeric mice compared to WT chimeras as early as 3 weeks post-transplantation (Fig. 3C-G), thereby indicating cell-extrinsic Cxcr4-mediated regulation of the skeletal landscape. Likewise, cortical bone content was slightly affected (Fig. 3H and 3I). Altogether, these findings suggest that impaired Cxcr4 desensitization in both skeletal and hematopoietic cells have combinatorial effects on bone landscape dysregulation in adult *Cxcr4*^{1013}-bearing mice.

Increased bone resorption and reduced bone formation in *Cxcr4*^{1013}-bearing mice

Bone is maintained by coupled activities of bone-forming OBLs and bone-resorbing osteoclasts (OCLs). Alterations in bone balance can result in pathologic bone loss and osteoporosis. This led us to investigate whether the gain-of-*Cxcr4*-function mutation modulates the OBL/OCL balance. First, we analyzed bone resorption by quantifying OCL numbers in mice using Tartrate Resistant Acid Phosphatase (TRAP) staining[61]. We observed increased OCL surface (Oc.S/BS) and number (Oc.N/BV) in mutant mice compared to WT ones (Fig. 4A and 4B). To determine whether the increased bone resorption in mutant mice resulted from OCL-intrinsic defects, we performed *in vitro* OCL differentiation from BM cells in the presence of M-Csf and Rank-L and tested their bone resorption capacity. Similar OCL numbers and bone matrix resorption activities were observed among WT and mutant cultures (Fig. S2A and S2B), suggesting preserved intrinsic capacities of mutant BM myeloid cells to differentiate *in vitro* into functional OCLs. Congruent with this, we observed no changes in expression levels of osteoclastogenic genes in mutant cultures compared to WT ones (Fig. S2C). These findings indicate that the *Cxcr4* mutation does not affect *in vitro* OCL differentiation and function but suggest that osteoclastogenesis and increased bone resorption in mutant mice may be promoted by the BM environment.

Cxcr4^{1013}-bearing mice exhibited similar bone formation as revealed by osteoid surface (OS/BS) and osteoblast surface (Obl.S/BS) compared to WT mice (Fig. 4C). Dynamic parameters of *in vivo* bone formation were also assessed by quantifying bone surfaces labelled with tetracycline and calcein. Total and double labelled surfaces were lower in mutant than WT mice (Fig. 4D), whilst mineral apposition rate (MAR) were similar in WT and *Cxcr4*^{1013}-bearing mice (Fig. 4E). Overall, bone formation rate (BFR/BS) was significantly reduced in mutant mice (Fig. 4E). This suggests a decrease in bone formation related to a lower number of OPCs and OBLs with maintained activity of individual OBL. In line with preserved intrinsic bone formation capacities of active osteoblastic lineage cells in mutant mice, high-throughput RNA sequencing (RNA-seq) and qPCR analyses of OPC bulk-sorted by flow cytometry from the bone fraction on the basis of the CD51 and Sca-1 markers (Fig. 2A) highlighted a gene signature with preserved mineralized matrix potential in mutant OPCs (Fig. 4F-H and S2D-F). In agreement, sorted OPCs from mutant mice were as efficient as WT ones *in vitro* at producing differentiated OBLs and mineralized nodules after 14- or 21-days culture in osteogenic medium as determined by Alkaline phosphatase (Alp) and Alizarin Red (AR) staining respectively[24,60,62,63] (Fig. 4I and S2G). This was confirmed by qPCR analyses with no changes in expression of genes encoding osteogenic regulators in mutant cultures (Fig. S2H). These findings suggest reduced osteogenic lineage commitment in *Cxcr4*^{1013}-bearing mice. Given that osteogenic cells support osteoclastogenesis through the production of factors such as Rank-L (*Tnfsf11*)[64], we questioned our RNAseq data on the related gene expression profile in mutant and WT OPCs. No major changes in expression levels of pro-osteoclastogenic or anti-resorptive genes were revealed in mutant OPCs (Fig. 4J and 4K).

To investigate whether increase in OCLs in mutant mice is linked to an altered stromal BM environment, we sought to set up co-culture experiments between *in vitro* expanded osteogenic cells carrying or not the *Cxcr4* mutation and WT OCL precursors, *ie.*, BM CD11b^{+}

myeloid cells as reported[65]. We showed that mutant osteogenic cells promoted exacerbated OCL differentiation compared to WT cells (Fig. 4L). Soluble factors seem not to be sufficient as the supernatants of such stimulated expanded osteogenic cells (WT or mutant) did not induce OCL differentiation. Additionally, transcriptomic analyses of stimulated osteogenic cells carrying or not the *Cxcr4* mutation did not reveal any major changes in expression levels of master genes regulating osteoclastogenesis (Fig. 4M). These findings suggest a juxtacrine function of osteogenic cells toward OCL differentiation that likely relies on direct interactions between both cell types and involves the Cxcl12/Cxcr4 axis.

Taken as a whole, our findings suggest that the hematopoietic contribution to bone loss in *Cxcr4*^{1013}-bearing mice likely involves dysregulation of the OCL compartment regardless of their activity. The overall decrease in bone mass in mutant mice may involve modulation of osteogenic and osteoclastogenic components with decreased bone formation and increased bone resorption. Bone remodeling involves a tight regulation of opposite processes leading to bone resorption and bone formation[66,67]. The observation that immature and mature osteogenic cells, *i.e.*, OPCs and OBLs, displayed preserved intrinsic functions led us to study the early differentiation process of the osteolineage.

Impaired osteogenic specification of *Cxcr4*^{1013}-bearing skeletal stromal cells

We thus investigated the intrinsic characteristics of SSCs carrying the *Cxcr4* mutation. Undifferentiated stem cells are characterized by their slow cell cycle progression in unperturbed conditions[9,68]. This led us to interrogate by flow cytometry the cycling status of SSCs from the bone fractions of *Cxcr4*^{1013}-bearing mice by performing DAPI/Ki-67 staining. A slight but significant increase in the frequency of cells in the quiescent G0 state (DAPI^{low}Ki-67^{-}) was observed among 1013/1013 SSCs but not in the more differentiated osteoblastic pool (Fig. 5A). The turnover of those cells was then studied by performing a 12-day BrdU pulse-chase assay

in vivo (Fig. 5B). Consistent with previous studies[28,69], the fraction of $BrdU^+$ cells in WT SSCs reached ~5%, while we observed a *Cxcr4*^{1013} allele copy number-dependent reduction in BrdU incorporation within mutant SSCs. No changes were observed among mutant OPCs compared to WT ones. Combined to reduced SSC and OPC numbers in mutant bones (Fig. 2B), these findings are suggestive of reduced cycling and osteogenic differentiation capacities of *Cxcr4*^{1013}-bearing SSCs.

To gain further mechanistic insights, we investigated the impact of the gain-of-Cxcr4-function on the molecular identity of SSCs by performing RNA-seq analyses of bulk-sorted SSCs from the bone fraction of WT and mutant mice. Biological processes related to cell cycle and osteogenic differentiation were significantly modulated in 1013/1013 SSCs as determined by Gene set enrichment analysis (GSEA) (Fig. 5C). The signature for genes related to cell cycle progression and regulation was reduced in 1013/1013 SSCs (Fig. S3A and S3B). Likewise, genes related to osteogenic differentiation appeared to be decreased in mutant SSCs (Fig. 5D and 5E). In contrast, key genes involved in both adipogenesis and chondrogenesis were not differentially expressed in mutant SSCs (Fig. S3C). These results were confirmed by microfluidic-based multiplex gene expression analyses (Fig. 5F and 5G and Fig. S3D), thus suggesting that proper Cxcr4 signaling is required for regulating osteogenic specification of SSCs. No changes in expression levels of pro-osteoclastogenic genes were detected in mutant SSCs compared to WT ones (Fig. 5H-J). Therefore, these results unravel a Cxcr4-mediated transcriptional signature in *Cxcr4*^{1013}-bearing SSCs suggestive of impaired cell cycle progression and defective osteogenic specification.

In adult BM, the majority of OBLs derives from OPCs identified by markers such as osterix (Osx)[3,9,17,28,70-72]. They are predominantly found close to the growth plate cartilage along trabecular bone of the primary spongiosa, and along the metaphyseal cortical bone[70,71,73]. We thus examined whether the gain-of-*Cxcr4*-function mutation alters the number of Osx-positive

OPCs by immunodetection on bone sections. We found fewer Osx-positive OPCs in mutant bones compared to WT (Fig. 5K and 5L). This decrease was confirmed by flow cytometry in the flushed stromal marrow fraction that encompasses Sca-1-negative and PDGFRα-positive early OPCs with multipotent adipo/osteogenic potential (Fig. 5M)[28,45,70]. Together, these data suggest that the decrease in early and committed OPCs in mutant mice may arise from a defect in osteogenic specification of BM-residing SSCs.

Cxcr4 desensitization intrinsically regulates *in vitro* the osteogenic differentiation of skeletal stromal cells

To assess whether Cxcr4 desensitization could regulate SSC fate toward the osteogenic lineage in a cell-intrinsic manner, we first compared *in vitro* the clonogenic capacities of WT and mutant total skeletal cells. There was a significant decrease in the number of colony-forming units-fibroblast (CFU-Fs) in mutant bone cell cultures that followed a *Cxcr4*^{1013} allele copy number-dependent pattern (Fig. 6A). These results suggested that impaired Cxcr4 signaling might affect *in vitro* overall SSC numbers as well as their proliferation. To test this, we evaluated by flow cytometry cell cycle and proliferation of SSCs expanded *in vitro* using BrdU, Cell Trace Violet (CTV) and DAPI/Ki-67 staining. By day 5 after BrdU pulse, we observed a *Cxcr4*^{1013} allele dose-dependent reduction in BrdU incorporation within mutant SSCs as compared to WT (Fig. 6B, left panel). Consistently, the fraction of proliferating CTV^{low} cells was reduced among mutant SSCs three days after loading (Fig. 6B, right panel). This altered proliferative capacity of *Cxcr4*^{1013}-bearing SSCs was associated with a slight but significant increase in proportions of SSCs in the quiescent G0 state (DAPI^{low}Ki-67^{-}), whereas no changes in apoptosis level were observed (Fig. 6C). This might account for the increased doubling time of mutant SSCs as well as their overall reduced number during the culture (Fig. 6D). Altogether,

these findings suggest that Cxcr4 desensitization is required *in vitro* for appropriate SSC proliferation, expansion and likely maintenance.

Next, we investigated *in vitro* the osteogenic potential capacities of *Cxcr4*^{1013}-bearing SSCs[62,63]. Staining of *in vitro* differentiated osteogenic cells and mineralization capacities by Alp and AR was significantly reduced in cultures from mutant SSCs in an allele dose-dependent manner (Fig. 6E and 6F, upper panels). Real-time PCR analysis revealed decreased expression of genes encoding osteogenic regulators in mutant cultures (Fig. 6G, upper panels). This was more marked for early osteogenic genes downstream the master regulator Runx2 such as *Osx* and particularly evident in the culture of 1013/1013 SSCs, thus suggesting defects at very early stages in the osteogenic differentiation process. In line with this, higher mRNA expression of *Sca1* and *Pdgfrα* was observed in mutant cultures three weeks after pro-osteogenic condition initiation (Fig. S4A, left panel). Consistent with the results obtained with Alcian blue and Perilipin staining on bone sections (Fig. 1G and 1H), *Cxcr4*^{1013}-bearing SSCs differentiated into adipocytes or chondrocytes similarly to WT SSCs when cultured *in vitro* with adipogenic or chondrogenic media respectively (Fig. S4B and S4C). Collectively, these data reveal *in vitro* a selective reduction of the osteogenic differentiation capacity of mutant SSCs, and further confirm a pivotal role for Cxcr4 desensitization in regulating this process at very early stages.

Normalization of Cxcr4 signaling rescues the osteogenic properties of *Cxcr4*^{1013}-bearing mouse skeletal cells

We then determined whether targeting Cxcr4 signaling would counteract the defective osteogenic fate of mutant SSCs. First, we assessed *in vitro* the impact of adding AMD3100 every 2 days on the osteogenic capacities of SSCs. AMD3100-mediated inhibition of Cxcr4 signaling in WT SSCs led to slight changes including decreased numbers of osteogenic cells (Fig. 6E and 6F, lower panels). By contrast, mutant cultures were highly sensitive to AMD3100

treatment as shown by the normalization of Alp and AR colorations 14 and 21 days after differentiation respectively (Fig. 6E and 6F) and of the expression of *Sca1* and *Pdgfrα* (Fig. S4A). Moreover, AMD3100-mediated reversion of defective osteogenesis within *Cxcr4*^{1013}-bearing SSC cultures was associated with normalized gene expression of osteogenic master regulators (Fig. 6G, lower panels), thus unravelling that Cxcr4 desensitization intrinsically regulates *in vitro* the osteogenic differentiation of SSCs.

Then, we assessed the impact of daily intraperitoneal injections for 3 weeks of 5 mg/kg AMD3100 on the bone landscape in adult WT and mutant mice (Fig. 7A). Cxcr4 inhibition decreased slightly the number of WT skeletal cells, and notably OPCs, in the bone fraction (Fig. 7B). In line with this, Opn-stained femoral sections revealed minor alterations in the architecture of WT mice trabecular microstructures upon treatment (Fig. 7C). This was extended to lumbar spine that displayed roughly normal BMD values in treated vs untreated WT mice (Fig. 7D). In 1013/1013 mice, chronic AMD3100 treatment reversed the quantitative defect in skeletal cells by normalizing the numbers of SSCs and OPCs (Fig. 7B). This was not evidenced in +/1013 mice nor associated with a rescue of the trabecular or the cortical network (Fig. 7C and 7E). However, AMD3100 treatment ameliorated slightly but significantly BMD values of lumbar spine in mutant mice (Fig. 7D), suggesting a correcting effect of Cxcr4-dependent signaling dampening on other cell types and mechanisms such as OCLs or LepR-positive BM SSCs as recently reported[31]. Therefore, these data suggest that integrity of Cxcr4 signaling is required for maintaining the osteogenic properties of skeletal cells.

BM stromal cells from WS patients displayed *in vitro* impaired osteogenic capacities

Finally, we sought to investigate if CXCR4 desensitization was mechanistically involved in regulating *in vitro* the multilineage differentiation capacities of human primary BMSCs that constitute a heterogeneous population containing skeletal progenitors[18]. To this end, we

analyzed BM samples from two unrelated patients with WS and carrying the heterozygous *CXCR4*^{R334X} mutation. In parallel, we expanded *in vitro* BMSCs from BM aspirates of seven independent healthy donors. All culture-expanded BMSCs were negative for the CD45 hematopoietic marker lineage but positive for CD73, CD90 and CD105, a combination of markers that are indicative of stromal/fibroblastic cells (Fig. S5A). Both healthy and WS BMSCs were spindle shaped and fibroblast-like cells and had the ability to form stromal colonies as shown by CFU-F assay (Fig. S5B and S5C). CXCL12 and its two receptors CXCR4 and ACKR3 were readily detectable and found at similar levels between cultured healthy and WS BMSCs (Fig. S5D-F). However, real-time PCR analyses revealed decreased expression of genes encoding early and late osteogenic master regulators in WS BMSC cultures compared to healthy controls (Fig. 8A). In line with this, when equal numbers of cells were plated at the start of the assay, WS BMSCs exhibited defective capacities to generate *in vitro* osteogenic progeny in contrast to BMSCs harvested from healthy donors (Fig. 8B). In contrast, WS BMSCs were as efficient as control cells to generate adipocytes in appropriate culture media condition (Fig. 8C). Therefore, these findings suggest that *in vitro* osteogenic differentiation of human primary BMSCs requires proper CXCR4 signaling regulation.

DISCUSSION

In this study, we investigated the regulatory role of CXCR4 signaling termination in the self-renewal and differentiation capacities of adult BM-residing SSCs. We used a knock-in mouse model expressing a naturally occurring WS-linked heterozygous gain-of-function *Cxcr4* mutation as well as human BM samples and clinical data from healthy and WS donors. We demonstrated a mutated allele dose-dependent effect of the WS-linked *Cxcr4*^{1013} mutation on trabecular bone microstructures mimicking an osteoporotic-like syndrome, evidenced as well in one quarter of WS patients. This Cxcr4-mediated reduction in bone content involved both cell-autonomous and cell-extrinsic defects in SSCs (Fig. 8D). Indeed, we provided unanticipated evidence that Cxcr4 desensitization is intrinsically required for regulating *in vitro* the quiescence/cycling balance of SSCs and preserving their osteogenic potential, while it was found to be dispensable for their adipogenic and chondrogenic differentiation. Some other BM cellular components contributed to the dysregulation of the bone phenotype. We observed in trabecular area an increase in OCL number. However, the osteoclastogenic differentiation potential of OCL precursors and the resorptive function of differentiated OCLs were not affected *in vitro* by the *Cxcr4*^{1013} mutation. Therefore, the osteopenia might proceed from a deregulated bone matrix resorption that might not be compensated enough by bone-forming cells, enlightening further the strong entanglement between both actors of bone remodeling. Unravelling the mechanisms leading to such an alteration of the skeletal landscape with a focus on the defective osteogenic capacities of SSCs driving the observed excessive bone defect will require further investigations using specific conditional mouse models. Importantly, defective osteogenic capacities were also evidenced *in vitro* in BMSCs from WS patients. These anomalies establish the C-tail of CXCR4 as an important regulatory domain of the receptor function in BM stromal cell biology in both mice and humans. In light of previous works[40,41,43,44], our results also suggest that both increased and decreased Cxcr4-mediated

signaling negatively impact skeletal stromal elements, thus indicating that fine-tuning of Cxcr4 signaling is critical for maintenance and osteogenic specification of adult SSCs. Although the underlying molecular mechanisms remain to be elucidated, Cxcr4 might act as a rheostat regulating the strength and kinetic of signaling pathways involved in osteogenic fate specification of SSCs. Interestingly, a recent work using a new mouse model of WS further illustrated the crucial role of fine-tuned Cxcr4-mediated signaling in mesenchymal stromal/stem cell (MSC) function[46]. Indeed, the lymphopoiesis process was reduced, as observed in our model[53], because of a dysregulated transcriptome in MSCs isolated from the flushed marrow fraction and characterized by a switch from an adipogenic to an osteolineage-prone program with limited lymphopoietic activity. This might proceed from reduced expression of IL-7 and excessive signaling through the lymphotoxin beta receptor in MSCs. Whether these changes are observed in the BM of our mouse model and how they would contribute to the bone loss warrant further investigations. Moreover, mice deficient for the gene encoding the transcription factor Ebf3 display an opposite BM phenotype to the one of *Cxcr4*^{1013}-bearing mice, characterized by osteosclerosis with HSC depletion and reduced expression of niche factors[69]. This was related to the uncontrolled ability of *Ebf3*-deficient SSCs to differentiate into OBLs. Further studies are required to address the status of Ebf3 and downstream target genes that act to modulate osteogenic fate of SSCs in *Cxcr4*^{1013}-bearing mice. A potential crosstalk between distinct SSC subsets, either prone to differentiate into osteochondro-lineage cells or perivascular and adipocyte lineage cells, has been reported[74]. This seems to imply ligand-receptor gene pairs such as TGFβ, WNT or BMP ligands and their cognate receptors that regulate SSC fate decision. Whether and how the Cxcl12/Cxcr4 signaling axis contributes to these regulatory mechanisms across SSC types remains also to be explored.

We reported that loss of Cxcr4 signaling termination impairs overall number, impedes cell cycle progression, and limits osteogenic differentiation of SSCs. Indeed, mutant mice have

a global alteration of the bone stromal landscape, including decreased numbers of SSCs and their progeny including early and committed OPCs and impaired architecture of trabecular and cortical bone microstructures that occurred in a mutated allele copy number-dependent manner. Altogether, these findings indicate that the gain-of-*Cxcr4*-function mutation promotes a reduced OBL commitment and differentiation, but does not alter the bone forming activity of individual OBL. Congruent with this, chronic treatment with AMD3100 normalized *in vitro* the osteogenic properties of mutant SSCs. Impaired Cxcr4 desensitization might alter the balance between quiescence and differentiation of mutant SSCs and reduce the number of osteogenic-endowed precursors. Currently, the prevailing view is that BM Cxcl12-expressing stromal cells display slow cell cycle progression and constitute an active source of trabecular and cortical OBLs under physiological conditions, as well as in response to injury[6,9,28,31,69]. We found a higher proportion of quiescent SSCs in mutant mice that was particularly evident in 1013/1013 SSCs, thus suggesting the importance of Cxcr4 desensitization in controlling SSC proliferation and quiescence and likely their capacity to give rise to osteogenic cells.

Loss of bone content in mutant mice was accompanied by a higher number of OCLs within the trabecular bones, possibly reflecting that the *Cxcr4* mutation was intrinsically perturbing the OCL differentiation process. This seems not to be the case since we showed that defective Cxcr4 desensitization did not increase *in vitro* differentiation of OCLs from mutant BM progenitors, nor their mineral matrix resorbing capacities. BM chimeras leading to a WT hematopoietic development into a mutant bone environment further ruled out the sole involvement of an uncontrolled bone resorption due to defective OCLs with excessive activity. These cells derive from monocytic lineage precursors upon stimulation by RankL and M-Csf[75,76]. In a constant cross interaction between the bone forming and the bone resorbing pathways, these osteoclastic cytokines are produced by mature and immature stromal cell populations within the BM[9,77,78]. While we did not observe increased *Rank-L*, *M-Csf* or *Opg*

(encoding a Rank-L antagonist) gene expression in sorted committed OPCs from mutant bones, we cannot exclude that modification of the bone stroma due to osteogenic defects might in turn modulate the production of osteoclastic factors from the mutant bone environment. Supporting this assumption, co-cultures of WT OCL progenitors with *in vitro* expanded *Cxcr4*^{1013}-bearing bone-derived stromal cells, stimulated to produce osteoclastogenic factors, led to enhanced osteoclastogenesis compared to WT stromal cells. No increase in *Rank-L* or *M-Csf* expression nor decrease in *Opg* level could be detected, suggesting the involvement of other additional mediators. It has recently been shown that intrinsic aging of SSCs resulted in higher proportion of stromal lineages producing pro-inflammatory and pro-resorptive factors, promoting myeloid skewing, and osteoclastic activity[30]. Whether a similar mechanism occurs in *Cxcr4*^{1013}-bearing mutant mice remains to be characterized. Moreover, BM chimeras leading to a mutant hematopoietic development into a WT bone environment displayed dysregulated bone landscape, thus emphasizing that transplanted hematopoietic cells can participate in bone loss through direct and/or indirect actions on osteoclastogenesis. Despite altered hematopoiesis in such chimeric mice, the myeloid skewing reported elsewhere[53] might account for excessive OCL number. As well, the reduced lymphopoiesis observed[46,53] still led to generation of mature B and T lymphocytes that are present in the BM and hence may act as potential actors in bone erosion as they can produce osteoclastogenic mediators such as Rank-L in non-physiological settings[79]. Whether such action of mutant hematopoietic donor cells recreates a pro-osteoclastogenic environment through a remodeling of the myeloid and lymphoid compartments deserves further investigations. Interestingly, the dysregulated bone landscape in BM chimeras with a mutant hematopoietic compartment in WT recipients was even stronger than that observed in mutant mice at steady-state. This observation raises the intriguing possibility of a pro-osteogenic effect of one or several *Cxcr4*^{1013}-bearing radioresistant cell

type(s). To test this possibility, further work will be required using mouse model where the mutation is carried in a cell-specific manner.

Osteogenesis is regulated, among different mechanisms, by undifferentiated skeletal cells and more specified osteolineage cells that express factors promoting or preventing their own differentiation into OBLs[23,59,69,80]. In BM, HSPC niches constitute critical spatio-temporal regulatory units composed of multiple cell populations of hematopoietic and non-hematopoietic origin cross-interacting with each other's in a dynamic setting[1,3,9,81,82]. This implies that immune and vascular cells among others may influence the osteogenic differentiation process[83]. Again, in BM chimeras in which *Cxcr4*^{1013}-bearing HSPCs were differentiating into a WT bone environment, we reported a similar bone loss as observed in mutant mice, thus indicating cell-extrinsic Cxcr4-mediated regulation of the skeletal landscape. This also suggests that neither the epiphyseal cartilage nor any developmental defect contribute to impaired trabecular bone architecture in adult mutant mice, and further supports the notion that HSPCs, as osteolineage cells do, express regulating osteogenic factors such as BMP-2, BMP-7 and WNT3a, that are particularly involved in SSC osteogenesis specification[17]. Whether and how hematopoietic cells, or other BM components such as vascular cells, participate in the defective osteolineage specification of SSCs in *Cxcr4*^{1013}-bearing mice deserves further investigations.

Finally, we reported that five out of nineteen patients with WS and carrying distinct autosomal-dominant mutations in *CXCR4* exhibit a decrease in BMD at different anatomical sites. Although this would merit to be extended to a larger cohort before introducing any potential bone-affecting drugs, these data suggest that accelerated osteopenia/osteoporosis and increased risk of fractures may constitute a novel feature of WS. Lack of CXCR4 desensitization could be mechanistically involved in such anomaly since BMSCs from WS patients carrying a heterozygous *CXCR4* mutation displayed *in vitro* impaired capacities to differentiate into osteogenic, but not adipogenic, cells. Strikingly, we observed that chondro-

and adipo-genic differentiation of murine mutant SSCs was normal both *in situ* and *in vitro*. Considering recent studies unraveling human SSCs expressing the CXCL12/CXCR4 axis with osteoblastogenic and, depending on their tissue origin, adipocytic potential[18,84], our findings pave the way for exploring the BM of WS patients in search for potential defect(s) in these skeletal populations.

METHODS

Healthy and WS donors and bone mineral density measurements

Investigations of human BM samples were performed in compliance with Good Clinical Practices and the Declaration of Helsinki. The study was approved by the Ethical Board Ile-de-France X. Recruited WS patients were not compensated and gave their written informed consent for participating to the clinical study that has been approved by NIAID Institutional Review Board (IRB). Cryopreserved BM aspirates from two WS patient (NIH protocol 09-I-0200) were provided through a NIH Material Transfer Agreement. The samples were anonymized. BM samples from seven healthy donors that were matched for age and sex and used as control subjects were isolated from hip replacement surgery samples (Protocol 17-030, n° ID-RCB: 2017-A01019-44). Primary BMSCs from healthy and WS donors were amplified and used at passage 1 to 3. For BMD assessment, data were collected from nineteen WS patients as part of an IRB approved clinical protocol conducted at the NIH (NIAID Protocol #2014-I-0185, IND # 118767). Patients had a baseline bone density scan as part of a drug treatment trial (NCT02231879) comparing 1 year of twice daily filgrastim (Neupogen) versus plerixafor (Mozobil) in a randomized, blinded crossover design. There were 13 women and 6 men with an average age of 30.5 years (range 10-56). The samples were anonymized. Patients had been on filgrastim (Neupogen) for an average of 5.7 years prior to enrolling in the trial (range 0-27). 6 of the 19 had not used filgrastim regularly prior to trial enrollment. BMD values expressed as T- or Z-scores were measured by total body dual-energy X-ray absorptiometry with a Lunar iDXA densitometer (GE Healthcare). Five WS patients had abnormal screening bone density by WHO criteria, anonymized at the start of the Phase 3 trial (Table 1), while the other 14 patients had normal bone density.

Mice and genotyping

All mice were bred in our animal facility under a 12h light/dark cycle, specific pathogen-free conditions (EOPS status) and fed *ad libitum*. For breeding, mice were in conventional cages with filter top. For experimentation, mice were housed in individually ventilated cages. All experiments were performed in accordance with the European Union guide for the care and use of laboratory animals and have been reviewed and approved by institutional review committees (CEEA-26, Animal Care and Use Committee, Villejuif, France and Comité d'Ethique Paris-Nord/N°121, Paris, France). *Cxcr4*$^{+/1013}$ (+/1013) mice were generated by a knock-in strategy[51]. Homozygous *Cxcr4*$^{1013/1013}$(1013/1013) mice were obtained by crossing heterozygous +/1013 mice. WT mice were used as controls. Unless specified, all mice were littermates, females and age-matched (8-12 wk-old). Adult Boy/J (CD45.1) (Charles River) mice were used as BM donors. Daily observation was performed to ensure that no animal was left in a state of pain or suffering during experimentation. Euthanasia was performed by increasing gradient of CO_2.

Sample isolation in mice

Mouse SSCs were obtained from bones after centrifugation of intact femurs, tibias and hips to flush out the BM cells. Flushed long bones were cut into fine pieces before enzymatic digestion with 2.5 U/mL collagenase type I (Thermofisher) for 45 min at 37°C under agitation. Released cells were filtered and washed with PBS, 2% FBS (Fetal Bovine Serum). Cell numbers were standardized as total counts per two legs. Peripheral blood was collected by cardiac puncture. Freshly isolated cells were either immunophenotyped, incubated at 37°C for 60 min in RPMI 20 mM HEPES 0.5% BSA (Euromedex) prior to chemokine receptor internalization studies, or expanded in αMEM medium supplemented with 10% FBS, 1% P/S (penicillin 100 Units/mL, streptomycin 100 Units/mL, Gibco) and 50 µM β-mercaptoethanol (PAN biotech). For BMD quantification, lumbar spines were fixed overnight in ethanol 70° and analyzed by dual-energy

X-ray absorptiometry with an ultrafocus DXA densitometer (Faxitron). Quantifications were made on a ROI of 2 lumbar spines.

Flow-cytometric analyses

Mouse and human staining analyses were carried out on an LSRII Fortessa flow cytometer (BD Biosciences) using the antibodies (Abs) described in Table S1. A Live/Dead Fixable Aqua Dead Cell Stain Kit (Biolegend) was used. To assess the compartmentalization of CXCR4 and ACKR3, human BMSCs were incubated with saturating concentrations of non-conjugated mouse anti-human CXCR4 or ACKR3 Abs, washed in PBS, fixed and permeabilized using the BD Cytofix/Cytoperm Fixation/Permeabilization Kit (BD Biosciences). BMSCs were subsequently stained with anti-CXCR4 and -ACKR3 conjugated mAbs, or the corresponding isotype control, at 4°C for 30 min and then analyzed by flow cytometry. FACS Diva software version 7 (BD) were used for collecting data. FLOWJO v10.7 (BD) and GraphPad Prism v8.0e (GraphPad software Inc.) were used for analyzing flow cytometric data.

***In vitro* functional assays**

Mouse CFU-Fs were performed by plating $1x10^5$ bone cells at passage 2-3 from WT and mutant mice. Human CFU-Fs were performed by plating 0.2 x 10^3 BMSCs into a 25 cm^2 flask at passage 3 from healthy or WS donors. After 7 or 10 days of culture, colonies were fixed with ethanol 70%, stained with 2% crystal violet (Sigma-Aldrich), and counted with a binocular magnifying glass. For chemotaxis assays, $5x10^4$ SSCs were added to the upper chambers of a 24-well plate with 8-µm-pore-size Transwell inserts (EMD Millipore) containing or not 1 nM Cxcl12 (R&D Systems) in the lower chamber. For inhibiting Cxcr4-mediated signaling, 10 µM AMD3100 (Sigma-Aldrich) was added in the upper and lower chambers. After 24h, membranes were removed and fixed in 4% paraformaldehyde (PFA). The cells that migrated to the lower

side of the membrane were stained with 0.1% crystal violet and three fields from each insert were counted under a light microscope. Cxcr4 and Ackr3 internalization assays were performed by incubating total bone cells at 37°C for 45 min with 10 nM Cxcl12. Then the reaction was stopped by adding ice-cold RPMI and quick centrifugation at 4°C. After one wash in acidic glycine buffer at pH= 4.3, levels of Cxcr4 and Ackr3 membrane expression were determined by flow cytometry. Cxcr4 or Ackr3 expression was calculated as follows: (Cxcr4 or Ackr3 geometric MFI of treated cells/Cxcr4 or Ackr3 geometric MFI of unstimulated cells) × 100; 100% corresponds to receptor expression at the surface of cells incubated in medium alone. For the chemokine scavenging assay, cultured SSCs were harvested by trypsinization and placed in complete medium for 90 min at 37°C and 5% CO_2 to normalize receptor expression. $4x10^6$ cells/mL were pre-incubated with 100 µM CCX733, a functional Ackr3 antagonist or vehicle in 1% BSA/PBS for 45 min at room temperature (RT). Then, $2x10^6$ cells/mL were incubated in presence of 5 nM AF647-Cxcl12 (Almac) in 1% BSA/PBS during 45-60 min at 37°C to allow internalization or on ice to inhibit this process. Cells were washed with 1% BSA/PBS and then either treated with an acidic glycine wash buffer pH= 2.7 for 3 min to dissociate cell-surface-bound chemokine, or washed with PBS to estimate internalized plus cell-surface-bound control. AF647 fluorescence (geometric MFI) was determined by flow cytometry. Phosphoflow assays were performed with the PerFix EXPOSE kit (Beckman coulter) on cultured SSCs and an anti-phospho Erk (pT202/pY204) was used. Fold change was calculated as follows: (Phospho-Erk geometric MFI of stimulated cells/Phospho-Erk geometric MFI of unstimulated cells).

In vivo **functional assays**

For BM transplantation experiments, $1.5x10^6$ total marrow cells from young $CD45.1^+$ WT mice were injected i.v. into lethally irradiated (two rounds of 5.5 Gy separated by 3 h) young $CD45.2^+$ WT, +/1013 or 1013/1013 recipient mice. For reverse experiments, $1.5x10^6$ total marrow cells

603 from CD45.2^{+} WT, +/1013 or 1013/1013 mice were injected into lethally irradiated CD45.1^{+}
604 WT recipient mice. Chimerism was analyzed 3 or 16 weeks after transplantation. For Cxcr4
605 blockade experiments, mice were daily injected intraperitoneally with 5 mg/kg AMD3100 or
606 PBS during 3 weeks. BM were harvested 2 h after the last injection and analyzed by flow
607 cytometry and imaging.
608
609 **ELISA**
610 Supernatants of culture-expanded human BMSCs were analyzed using a standardized ELISA
611 for human Cxcl12 (Quantikine; R&D Systems).
612
613 **Bone immunostaining and histomorphometry**
614 Mouse bones were fixed in 4% PFA overnight followed by one-week decalcification in EDTA
615 (0.5 M) at pH 7.4 under agitation. Bones were incubated in PBS with 20% sucrose and 2%
616 polyvinylpyrrolidone (PVP) (Sigma) at 4°C overnight and then embedded in PBS with 20%
617 sucrose, 2% PVP and 8% gelatin (Sigma) before storage at -80°C. Sections of 30 µm-thick
618 were rehydrated in PBS 1X, incubated 20 min at RT in PBS with 0.3% triton X-100, saturated
619 in blocking solution (PBS with 5% BSA) and finally incubated with primary Abs (Table S2).
620 After washing, secondary Abs were incubated for 1h at RT with DAPI for nuclear staining and
621 mounting using Permafluor mounting medium (Thermofisher). Images were acquired using
622 TCS SP8 confocal microscope and processed using Fiji software. For alcian blue and perilipin
623 A staining, fixed and decalcified femur bones were embedded in paraffin, sectioned (7 µm-
624 thick) and deparaffinized with xylene. Staining of cartilage tissues was performed with a 1 %
625 alcian blue solution for 30 min. Images were acquired using a LEICA DM4000B microscope
626 equipped with a DFC425C camera and processed with the Leica Application Suite V3.8
627 software. For perilipin A staining, heat induced epitope retrieval was performed in citrate

sodium buffer solution. Sections were saturated for 1h in PBS 1% BSA at RT, washed in PBS 0.2% BSA and 0.1% Triton X-100, and incubated with anti-perilipin A Ab in PBS BSA 1% overnight at 4°C. After washing, sections were incubated with TRITC-coupled rabbit anti-guinea pig Ab in PBS 1% BSA for 45 min and counterstained with DAPI. For Osx staining, 16 µm frozen sections were permeabilized in TBS-0.3% Triton X-100 for 10 min and blocked in TBS-2.5% BSA-2.5% Donkey Serum for 1h at RT. Sections were incubated with anti-Osx Ab (rabbit, Santa Cruz SC-22536R) in blocking solution overnight at 4°C. After washing with TBS+0.025% Triton X-100, sections were incubated in donkey anti-rabbit secondary Ab dylight 550 (SA5-10039, invitrogen) in blocking solution. After washing, sections were incubated 15 min at RT in DAPI at 0.1µg/mL prior to mounting in GB-Mount (Diagomics). Image acquisitions were done using the ApoTome optical sectioning system (Zeiss) with an inverted microscope (Zeiss Axio Observer Z1). Osx quantification was performed using the ICY software. For human BMSC immunofluorescence studies, cells were plated on coverslips and fixed with 4% PFA in PBS. Fixed cells were permeabilized with Triton X 0.3% for 10 min, blocked with PBS 5% BSA, 5% goat serum and incubated with unlabeled primary CXCL12 mAb overnight at 4°C followed by secondary AF633-coupled goat anti-mouse polyclonal Ab (Invitrogen) and the nuclear dye Hoechst 33342. Images were obtained with a Plan-Apochromatic objective using the LSM800 confocal microscope (Carl Zeiss). Sections were acquired as serial z stacks (0.39 µm apart) and were subjected to three-dimensional reconstruction (Zen 2.3 System).

Bone histomorphometry was performed in plastic samples, allowing the measurements of bone formation and resorption parameters. Mouse femurs were fixed in ethanol 70°, dehydrated and embedded in methyl methacrylate resin. Five micrometer-thick coronal sections were cut parallel to the long axis of the femur using an SM2500S microtome (Leica, Germany). Sections were deplastified, rehydrated and stained with toluidine blue or with naphthol 3-

hydroxy-2-naphthoic acid 4-chloro-2-methylanilide (ASTR phosphate, Sigma, St Louis, France) for detecting mature osteoclasts with TRAP staining. Quantifications were made on a polarizing microscope (Nikon) using a software package (Bonolab) developed for bone histomorphometry (Microvision, France). To allow the measure of dynamic parameters of bone formation, mice were intraperitoneally injected with tetracycline (20 mg/kg) and calcein (10 mg/kg; Sigma) 5 days and 1 day respectively before being killed. Two 12-µm-thick unstained sections were taken for measurement of the dynamic parameters under UV light. The matrix apposition rate (MAR) was measured using the Microvision image analyzer by a semiautomatic method using tetracycline and calcein double-labeled bone surfaces. The mineralizing surfaces (MS/BS) were measured in the same areas using the objective eyepiece Leitz integrate plate II. When specified, the cortical thickness was measured in paraffin-embedded sections stained with Toluidine Blue. The 2 cortices were measured using histomorphometry software and expressed as mean of both cortices for each sample. All the histomorphometric parameters were recorded in compliance with the recommendation of the American Society for Bone and Mineral Research Histomorphometry Nomenclature Committee. Five to six animals per genotype were analyzed by two different investigators.

Bone structure analysis by micro-computed tomography

Femurs were collected for bone microarchitecture analysis after fixation and before decalcification. They were analyzed with high-resolution microcomputed tomography (micro-CT) using a Skyscan 1272 microCT (SkyScan, Kontich, Belgium). Measurements were made on the femurs using the following acquisition parameters: voltage 60kV, pixel size 6µm, Filter Alu + 0.5mm. After 3-dimensional images reconstruction with NRecon®, analyses were performed on the trabecular and cortical region (1.72 mm and 0.43 mm thickness, respectively). Morphometric parameters such as Bone Volume/Tissue volume (BV/TV, %), Trabecular

number (Tb.Nb, 1/mm), Trabecular Separation (Tb.Sp, mm), Cortical Bone Volume (Ct.BV, mm^3) and Cortical Thickness (Ct.Th, mm) were assessed.

Cell culture and differentiation

Mouse osteoblastic differentiation was performed for 3 weeks in α-MEM medium with 10% FBS, 1% P/S, 50 µM β-mercaptoethanol supplemented with 50 µg/mL L-ascorbic acid and 10 mM glycerophosphate (Sigma) either from SSCs or sorted OPCs. Alkaline phosphatase staining was performed after 14 days of differentiation according to the Alkaline phosphatase Kit (Sigma). At day 21, cultures were fixed with 4% PFA, stained with alizarin red and quantified using the Osteogenesis assay kit (Millipore). When specified, AMD3100 (*versus* vehicle) was added into the osteogenic medium every 2 days at 10 µM respectively. Chondro- and adipogenic differentiations of SSCs were performed according to the StemPro-Chondrogenesis or -Adipogenic Differentiation Kits (ThermoFisher) for 2 weeks. After fixation, cells were treated with either Alcian Blue 1% (Sigma) to stain chondrocyte matrix or Oil Red O solution (Sigma) to reveal lipid droplets. For *in vitro* human osteogenic differentiation assays, expanded BMSCs were seeded at 3 x 10^3 *per* cm^2 in α-MEM supplemented with 10% FBS and 1% antibiotics. After cell adhesion, medium was replaced by α-MEM supplemented with 10% FBS, 1% antibiotics and 0.1 µM dexamethasone, 0.05 mM L-ascorbic acid-2-phosphate and 10 mM β-glycerophosphate. Medium was changed every 2 days during 3 weeks. Quantification of mineralization was performed after Alizarin Red S staining[85]. Human adipogenic differentiation assays were performed as described for the murine ones.

Osteoclast differentiation and functional analysis

OCLs were differentiated *in vitro*[86]. Briefly, 2.3 x 10^5 BM cells/cm^2 were plated in MEM-alpha (ThermoFisher) complemented with 5% serum (Hyclone, GE Healthcare), 1% P/S, 50 µM 2-

mercaptoethanol, 25 ng/ml M-Csf and 30 ng/ml Rank-L (R&D Systems). OCL differentiation (multinucleated $TRAP^+$ cells) was quantified at day 5 after TRAP coloration using the leukocyte acid phosphatase kit (Sigma). Matrix dissolution activity was evaluated by seeding a total of $2x10^4$ differentiated OCLs on 96-well osteoassay plates (Corning) in α-MEM containing 10% FBS and 30 ng/ml Rank-L. After 3 days, medium was removed and cells were detached by the addition of water. Resorbed areas were quantified using Fiji/ImageJ software[87].

Co-culture assays between osteogenic cells and osteoclast precursors

Mouse osteogenic cells were isolated from the bone fraction of WT or mutant mice as indicated above. They were expanded in α-MEM medium with 10% FBS, 1% P/S, 50 µM β-mercaptoethanol for 2 weeks, passaged and plated in 96-well plates (2×10^4 cells/well). Osteoclast precursors were obtained from $CD11b^+$-enriched cells (with CD11b-Microbeads, Milteniy Biotec, France) from the flushed marrow fraction of WT mice as previously described[86]. They were added, in co-culture, to WT or mutant expanded osteogenic cells (5×10^4 cell/well) and stimulated with 1,25-dihydroxy vitamin D3 (vitD3, 10 nM), prostaglandin E2 (PGE2, 1 µM) and Dexamethasone (Dex, 50 nM) as previously described[65] in order to stimulate osteogenic cells to produce RankL/MCSF and to inhibit OPG production[88,89]. OCL differentiation (multinucleated $TRAP^+$ cells) was quantified at day 8 after TRAP coloration as indicated above.

Cell cycle, viability, survival and proliferation assays

For flow cytometry-based cell cycle analyses, bone cells were permeabilized, fixed with the FOXP3 permeabilization kit (Foxp3/Transcription Factor Staining Buffer Set; eBioscience) and labelled with a Ki67 Ab and DAPI. For BrdU assays, mice were injected intraperitoneally with 180 µg BrdU (Sigma) and maintained with drinking water containing 800 µg/ml BrdU and 1%

glucose over 12 days. The BrdU labelling was analyzed by flow cytometry using the BrdU-FITC labeling kit (BD Biosciences). For *in vitro* BrdU incorporation, 3 µg/ml of BrdU was added to the culture and after five days the percentage of incorporation was determined as above. Apoptosis was measured using the Annexin V detection kit (BD Biosciences) with DAPI staining. For *in vitro* proliferation assays, SSCs were detached with 0.5% trypsin and loaded at 3 x 10^4 cells/well with cell trace violet (CTV, Thermofisher) for 15 min at 37°C. CTV dilution was assessed by flow cytometry. To estimate the doubling time values, SSCs were seeded at 3x10^3 cells/cm^2 and counted after 3 days of culture. The doubling time was calculated as follows: (time of culture x log(2))/(log(final number of SSC)-log(initial number of SSC)).

Quantitative real time-PCR

For mouse gene expression, total RNA was isolated from cultured or sorted SSCs and OPCs using the RNeasy Plus Mini or Micro Kit (Qiagen) and reverse transcribed with oligo(dT) and SuperScript II Reverse Transcriptase (Invitrogen). Quantitative RT-PCR reactions were performed on a Light Cycler instrument (LC480, Roche Diagnostics) with the LightCycler 480 SYBR Green detection kit (Roche Diagnostics) using primers reported in Table S3. For human gene expression, total RNA was isolated from cultured BMSCs using Trizol Reagent (ThermoFisher). Reverse transcription was performed using SuperScriptVilo IV (ThermoFisher). When required, total RNA from WS BMSCs and their related controls were extracted from 0.2 x 10^3 BMSCs and pre-amplified using CellsDirect One-Step qRT–PCR kit (Invitrogen). PCR reactions were performed using primers reported in Table S3 with Power SYBRGreen (Applied Biosystems) on a 7500 FAST apparatus (Applied Biosystems). Mouse *β-actin* and *36b4* and human *β-ACTIN* and *GAPDH* were used as standards for normalization. Relative quantification was determined by the comparative delta-Ct ($2^{-\Delta CT}$) method (fold

752 changes calculated relative to house-keeping genes) or delta-delta-Ct ($2^{-\Delta\Delta CT}$) method (fold
753 changes calculated by setting the mean values obtained from WT cells as one).
754
755 **Multiplex qPCR**
756 Multiplex qPCR was performed using the microfluidic Biomark system. One hundred SSCs
757 were sorted into PCR tubes containing 5 µl of reverse transcription/pre-amplification mix
758 containing 2X reaction buffer, SuperScriptIII from the CellsDirect One-Step qRT–PCR kit and
759 0.2X Taqman assay (Life technologies) (Table S4). cDNA pre-amplification was performed
760 during 22 cycles and pre-amplified product was diluted 1:5 in TE buffer before processing with
761 Dynamic Array protocol (Fluidigm). Cells expressing *β-actin* and control genes (*Runx2*, *Col1α*,
762 *Alp* and *Ibsp*) and not *Pax5* and/or *Cd3* (negative controls) were considered for analyses.
763 Expression of *β-actin* was used for normalization. Heatmaps were generated with
764 http://www.heatmapper.ca using Z scores.
765
766 **RNA sequencing**
767 Pools of 3 x 10^3 SSCs or OPCs were sorted from the bone fraction into RLT buffer (Qiagen)
768 with 1% of β-mercaptoethanol. RNA was isolated using RNeasy Micro Kit. cDNAs were
769 generated from 400 to 1,000 pg of total RNA using Clontech SMART-Seq v4 Ultra Low Input
770 RNA kit for Sequencing (Takara Bio Europe) and amplified with 12 cycles of PCR by Seq-
771 Amp polymerase. For Tn5 transposon tagmentation, 600 pg of pre-amplified cDNAs were used
772 by the Nextera XT DNA Library Preparation Kit (96 samples) (Illumina) followed by library
773 amplification of 12 cycles. Purification was performed with Agencourt AMPure XP and
774 SPRIselect beads (Beckman-Coulter). Sequencing reads were generated, in Paired-End mode,
775 on the GenomEast platform (Illumina). FastQC program was used to evaluate the quality of the
776 raw sequencing data and reads shorter than 50 bp were removed. Reads were aligned to the *Mus*

777 *musculus* genome (mm10 build) using the Star tool[90]. Gene expression quantification was
778 obtained using read counting software Htseq[91]. Normalization and differential analysis were
779 carried out with DESeq2 package by applying the Benjamini-Hochberg FDR correction ($p <$
780 0.05; 1.5-fold) for comparison between samples. Heatmaps and volcano plots were obtained
781 using the web server Heatmapper and EnhancedVolcano packages respectively.
782
783 **Statistics**
784 All statistical analyses were conducted using Prism software (GraphPad Software). A Kruskal-
785 Wallis test was used to determine the significance of the difference between means of WT,
786 +/1013 and 1013/1013 groups. Unless specified, the unpaired two-tailed Student *t* test was used
787 to compare means among two groups.
788
789 **DATA AVAILABILITY**
790 RNA-seq data that support the findings of this study have been deposited in the Gene
791 Expression Omnibus repository with the accession code GSE217422
792 (https://www.ncbi.nlm.nih.gov/geo/query/acc.cgi?acc=GSE217422). The data that support the
793 findings of this study are available from the corresponding author upon request. Source data
794 are provided with this paper.
795

REFERENCES

1. Wei, Q. & Frenette, P. S. Niches for Hematopoietic Stem Cells and Their Progeny. *Immunity* **48**, 632-648 (2018). https://doi.org:10.1016/j.immuni.2018.03.024

2. Bianco, P. Stem cells and bone: a historical perspective. *Bone* **70**, 2-9 (2015). https://doi.org:10.1016/j.bone.2014.08.011

3. Baryawno, N. *et al.* A Cellular Taxonomy of the Bone Marrow Stroma in Homeostasis and Leukemia. *Cell* **177**, 1915-1932 e1916 (2019). https://doi.org:10.1016/j.cell.2019.04.040

4. Grassinger, J., Haylock, D. N., Williams, B., Olsen, G. H. & Nilsson, S. K. Phenotypically identical hemopoietic stem cells isolated from different regions of bone marrow have different biologic potential. *Blood* **116**, 3185-3196 (2010). https://doi.org:10.1182/blood-2009-12-260703

5. Kiel, M. J. *et al.* SLAM family receptors distinguish hematopoietic stem and progenitor cells and reveal endothelial niches for stem cells. *Cell* **121**, 1109-1121 (2005). https://doi.org:10.1016/j.cell.2005.05.026

6. Nakahara, F. *et al.* Engineering a haematopoietic stem cell niche by revitalizing mesenchymal stromal cells. *Nat Cell Biol* **21**, 560-567 (2019). https://doi.org:10.1038/s41556-019-0308-3

7. Pinho, S. *et al.* Lineage-Biased Hematopoietic Stem Cells Are Regulated by Distinct Niches. *Dev Cell* **44**, 634-641 e634 (2018). https://doi.org:10.1016/j.devcel.2018.01.016

8. Sun, J. *et al.* Clonal dynamics of native haematopoiesis. *Nature* **514**, 322-327 (2014). https://doi.org:10.1038/nature13824

9. Tikhonova, A. N. *et al.* The bone marrow microenvironment at single-cell resolution. *Nature* **569**, 222-228 (2019). https://doi.org:10.1038/s41586-019-1104-8

10. Acar, M. *et al.* Deep imaging of bone marrow shows non-dividing stem cells are mainly perisinusoidal. *Nature* **526**, 126-130 (2015). https://doi.org:10.1038/nature15250

11. Asada, N., Takeishi, S. & Frenette, P. S. Complexity of bone marrow hematopoietic stem cell niche. *Int J Hematol* **106**, 45-54 (2017). https://doi.org:10.1007/s12185-017-2262-9

12. Balzano, M. *et al.* Nidogen-1 Contributes to the Interaction Network Involved in Pro-B Cell Retention in the Peri-sinusoidal Hematopoietic Stem Cell Niche. *Cell Rep* **26**, 3257-3271 e3258 (2019). https://doi.org:10.1016/j.celrep.2019.02.065

13. Comazzetto, S. *et al.* Restricted Hematopoietic Progenitors and Erythropoiesis Require SCF from Leptin Receptor+ Niche Cells in the Bone Marrow. *Cell Stem Cell* **24**, 477-486 e476 (2019). https://doi.org:10.1016/j.stem.2018.11.022

14. Ding, L., Saunders, T. L., Enikolopov, G. & Morrison, S. J. Endothelial and perivascular cells maintain haematopoietic stem cells. *Nature* **481**, 457-462 (2012). https://doi.org:10.1038/nature10783

15. Kunisaki, Y. *et al.* Arteriolar niches maintain haematopoietic stem cell quiescence. *Nature* **502**, 637-643 (2013). https://doi.org:10.1038/nature12612

16. Zhong, L. *et al.* Single cell transcriptomics identifies a unique adipose lineage cell population that regulates bone marrow environment. *Elife* **9** (2020). https://doi.org:10.7554/eLife.54695

17. Chan, C. K. *et al.* Identification and specification of the mouse skeletal stem cell. *Cell* **160**, 285-298 (2015). https://doi.org:10.1016/j.cell.2014.12.002

18. Chan, C. K. F. *et al.* Identification of the Human Skeletal Stem Cell. *Cell* **175**, 43-56 e21 (2018). https://doi.org:10.1016/j.cell.2018.07.029

19. Worthley, D. L. *et al.* Gremlin 1 identifies a skeletal stem cell with bone, cartilage, and reticular stromal potential. *Cell* **160**, 269-284 (2015). https://doi.org:10.1016/j.cell.2014.11.042

20. Calvi, L. M. *et al.* Osteoblastic cells regulate the haematopoietic stem cell niche. *Nature* **425**, 841-846 (2003).

21. Greenbaum, A. *et al.* CXCL12 in early mesenchymal progenitors is required for haematopoietic stem-cell maintenance. *Nature* **495**, 227-230 (2013). https://doi.org:10.1038/nature11926

22. Jung, Y. *et al.* Hematopoietic stem cells regulate mesenchymal stromal cell induction into osteoblasts thereby participating in the formation of the stem cell niche. *Stem Cells* **26**, 2042-2051 (2008). https://doi.org:10.1634/stemcells.2008-0149

23. Mendez-Ferrer, S. *et al.* Mesenchymal and haematopoietic stem cells form a unique bone marrow niche. *Nature* **466**, 829-834 (2010). https://doi.org:10.1038/nature09262

24. Nakamura, Y. *et al.* Isolation and characterization of endosteal niche cell populations that regulate hematopoietic stem cells. *Blood* **116**, 1422-1432 (2010). https://doi.org:10.1182/blood-2009-08-239194

25. Omatsu, Y. *et al.* The essential functions of adipo-osteogenic progenitors as the hematopoietic stem and progenitor cell niche. *Immunity* **33**, 387-399 (2010). https://doi.org:10.1016/j.immuni.2010.08.017

26. Yoshihara, H. *et al.* Thrombopoietin/MPL signaling regulates hematopoietic stem cell quiescence and interaction with the osteoblastic niche. *Cell Stem Cell* **1**, 685-697 (2007). https://doi.org:10.1016/j.stem.2007.10.020

27. Zhang, J. *et al.* Identification of the haematopoietic stem cell niche and control of the niche size. *Nature* **425**, 836-841 (2003).

867 28. Zhou, B. O., Yue, R., Murphy, M. M., Peyer, J. G. & Morrison, S. J. Leptin-receptor-
868 expressing mesenchymal stromal cells represent the main source of bone formed by
869 adult bone marrow. *Cell Stem Cell* **15**, 154-168 (2014).
870 https://doi.org:10.1016/j.stem.2014.06.008
871 29. Wolock, S. L. *et al.* Mapping Distinct Bone Marrow Niche Populations and Their
872 Differentiation Paths. *Cell Rep* **28**, 302-311 e305 (2019).
873 https://doi.org:10.1016/j.celrep.2019.06.031
874 30. Ambrosi, T. H. *et al.* Aged skeletal stem cells generate an inflammatory degenerative niche.
875 *Nature* **597**, 256-262 (2021). https://doi.org:10.1038/s41586-021-03795-7
876 31. Jeffery, E. C., Mann, T. L. A., Pool, J. A., Zhao, Z. & Morrison, S. J. Bone marrow and
877 periosteal skeletal stem/progenitor cells make distinct contributions to bone
878 maintenance and repair. *Cell Stem Cell* (2022).
879 https://doi.org:10.1016/j.stem.2022.10.002
880 32. Ara, T. *et al.* Long-term hematopoietic stem cells require stromal cell-derived factor-1 for
881 colonizing bone marrow during ontogeny. *Immunity* **19**, 257-267 (2003).
882 https://doi.org:10.1016/s1074-7613(03)00201-2
883 33. Cordeiro Gomes, A. *et al.* Hematopoietic Stem Cell Niches Produce Lineage-Instructive
884 Signals to Control Multipotent Progenitor Differentiation. *Immunity* **45**, 1219-1231
885 (2016). https://doi.org:10.1016/j.immuni.2016.11.004
886 34. Itkin, T. *et al.* Distinct bone marrow blood vessels differentially regulate haematopoiesis.
887 *Nature* **532**, 323-328 (2016). https://doi.org:10.1038/nature17624
888 35. Nie, Y., Han, Y. C. & Zou, Y. R. CXCR4 is required for the quiescence of primitive
889 hematopoietic cells. *J Exp Med* **205**, 777-783 (2008).
890 https://doi.org:10.1084/jem.20072513

36. Sugiyama, T., Kohara, H., Noda, M. & Nagasawa, T. Maintenance of the hematopoietic stem cell pool by CXCL12-CXCR4 chemokine signaling in bone marrow stromal cell niches. *Immunity* **25**, 977-988 (2006).

37. Miao, R. *et al.* Competition between hematopoietic stem and progenitor cells controls hematopoietic stem cell compartment size. *Nat Commun* **13**, 4611 (2022). https://doi.org:10.1038/s41467-022-32228-w

38. Ding, L. & Morrison, S. J. Haematopoietic stem cells and early lymphoid progenitors occupy distinct bone marrow niches. *Nature* **495**, 231-235 (2013). https://doi.org:10.1038/nature11885

39. Agarwal, P. *et al.* Mesenchymal Niche-Specific Expression of Cxcl12 Controls Quiescence of Treatment-Resistant Leukemia Stem Cells. *Cell Stem Cell* **24**, 769-784 e766 (2019). https://doi.org:10.1016/j.stem.2019.02.018

40. Hosogane, N. *et al.* Stromal derived factor-1 regulates bone morphogenetic protein 2-induced osteogenic differentiation of primary mesenchymal stem cells. *Int J Biochem Cell Biol* **42**, 1132-1141 (2010). https://doi.org:10.1016/j.biocel.2010.03.020

41. Li, G. *et al.* Hypermethylation of microRNA-149 activates SDF-1/CXCR4 to promote osteogenic differentiation of mesenchymal stem cells. *J Cell Physiol* **234**, 23485-23494 (2019). https://doi.org:10.1002/jcp.28917

42. Shahnazari, M., Chu, V., Wronski, T. J., Nissenson, R. A. & Halloran, B. P. CXCL12/CXCR4 signaling in the osteoblast regulates the mesenchymal stem cell and osteoclast lineage populations. *FASEB J* **27**, 3505-3513 (2013). https://doi.org:10.1096/fj.12-225763

43. Tzeng, Y. S. *et al.* Imbalanced Osteogenesis and Adipogenesis in Mice Deficient in the Chemokine Cxcl12/Sdf1 in the Bone Mesenchymal Stem/Progenitor Cells. *J Bone Miner Res* **33**, 679-690 (2018). https://doi.org:10.1002/jbmr.3340

916 44. Zhu, W., Liang, G., Huang, Z., Doty, S. B. & Boskey, A. L. Conditional inactivation of the
917 CXCR4 receptor in osteoprecursors reduces postnatal bone formation due to impaired
918 osteoblast development. *J Biol Chem* **286**, 26794-26805 (2011).
919 https://doi.org:10.1074/jbc.M111.250985
920 45. Matsushita, Y. *et al.* A Wnt-mediated transformation of the bone marrow stromal cell
921 identity orchestrates skeletal regeneration. *Nat Commun* **11**, 332 (2020).
922 https://doi.org:10.1038/s41467-019-14029-w
923 46. Zehentmeier, S. *et al.* Dysregulated stem cell niches and altered lymphocyte recirculation
924 cause B and T cell lymphopenia in WHIM syndrome. *Sci Immunol* **7**, eabo3170 (2022).
925 https://doi.org:10.1126/sciimmunol.abo3170
926 47. Dotta, L., Tassone, L. & Badolato, R. Clinical and genetic features of Warts,
927 Hypogammaglobulinemia, Infections and Myelokathexis (WHIM) syndrome. *Curr Mol*
928 *Med* **11**, 317-325 (2011).
929 48. Kawai, T. & Malech, H. L. WHIM syndrome: congenital immune deficiency disease. *Curr*
930 *Opin Hematol* **16**, 20-26 (2009). https://doi.org:10.1097/MOH.0b013e32831ac557
931 49. Murphy, P. M. & Heusinkveld, L. Multisystem multitasking by CXCL12 and its receptors
932 CXCR4 and ACKR3. *Cytokine* **109**, 2-10 (2018).
933 https://doi.org:10.1016/j.cyto.2017.12.022
934 50. Hernandez, P. A. *et al.* Mutations in the chemokine receptor gene CXCR4 are associated
935 with WHIM syndrome, a combined immunodeficiency disease. *Nat Genet* **34**, 70-74
936 (2003). https://doi.org:10.1038/ng1149
937 51. Balabanian, K. *et al.* Proper desensitization of CXCR4 is required for lymphocyte
938 development and peripheral compartmentalization in mice. *Blood* **119**, 5722-5730
939 (2012). https://doi.org:10.1182/blood-2012-01-403378

940 52. Biajoux, V. *et al.* Efficient Plasma Cell Differentiation and Trafficking Require Cxcr4
941 Desensitization. *Cell Rep* **17**, 193-205 (2016).
942 https://doi.org:10.1016/j.celrep.2016.08.068
943 53. Freitas, C. *et al.* Lymphoid differentiation of hematopoietic stem cells requires efficient
944 Cxcr4 desensitization. *J Exp Med* **214**, 2023-2040 (2017).
945 https://doi.org:10.1084/jem.20160806
946 54. Alouche, N. *et al.* Hematologic disorder-associated Cxcr4 gain-of-function mutation leads
947 to uncontrolled extrafollicular immune response. *Blood* **137**, 3050-3063 (2021).
948 https://doi.org:10.1182/blood.2020007450
949 55. Haribabu, B. *et al.* Regulation of human chemokine receptors CXCR4. Role of
950 phosphorylation in desensitization and internalization. *J Biol Chem* **272**, 28726-28731
951 (1997). https://doi.org:10.1074/jbc.272.45.28726
952 56. Balabanian, K. *et al.* WHIM syndromes with different genetic anomalies are accounted for
953 by impaired CXCR4 desensitization to CXCL12. *Blood* **105**, 2449-2457 (2005).
954 https://doi.org:10.1182/blood-2004-06-2289
955 57. Mayol, K., Biajoux, V., Marvel, J., Balabanian, K. & Walzer, T. Sequential desensitization
956 of CXCR4 and S1P5 controls natural killer cell trafficking. *Blood* **118**, 4863-4871
957 (2011). https://doi.org:10.1182/blood-2011-06-362574
958 58. Matsushita, Y., Ono, W. & Ono, N. Flow Cytometry-Based Analysis of the Mouse Bone
959 Marrow Stromal and Perivascular Compartment. *Methods Mol Biol* **2308**, 83-94 (2021).
960 https://doi.org:10.1007/978-1-0716-1425-9_7
961 59. Mende, N. *et al.* Prospective isolation of nonhematopoietic cells of the niche and their
962 differential molecular interactions with HSCs. *Blood* **134**, 1214-1226 (2019).
963 https://doi.org:10.1182/blood.2019000176

964 60. Morikawa, S. *et al.* Prospective identification, isolation, and systemic transplantation of
965 multipotent mesenchymal stem cells in murine bone marrow. *J Exp Med* **206**, 2483-
966 2496 (2009). https://doi.org:10.1084/jem.20091046
967 61. Parfitt, A. M. Osteoclast precursors as leukocytes: importance of the area code. *Bone* **23**,
968 491-494 (1998). https://doi.org:10.1016/s8756-3282(98)00140-9
969 62. Zhu, H. *et al.* A protocol for isolation and culture of mesenchymal stem cells from mouse
970 compact bone. *Nat Protoc* **5**, 550-560 (2010). https://doi.org:10.1038/nprot.2009.238
971 63. Abou Nader, Z., Espeli, M., Balabanian, K. & Lemos, J. P. Culture, Expansion and
972 Differentiation of Mouse Bone-Derived Mesenchymal Stromal Cells. *Methods Mol Biol*
973 **2308**, 35-46 (2021). https://doi.org:10.1007/978-1-0716-1425-9_3
974 64. Wright, H. L., McCarthy, H. S., Middleton, J. & Marshall, M. J. RANK, RANKL and
975 osteoprotegerin in bone biology and disease. *Curr Rev Musculoskelet Med* **2**, 56-64
976 (2009). https://doi.org:10.1007/s12178-009-9046-7
977 65. Ciucci, T. *et al.* Bone marrow Th17 TNFalpha cells induce osteoclast differentiation, and
978 link bone destruction to IBD. *Gut* **64**, 1072-1081 (2015). https://doi.org:10.1136/gutjnl-
979 2014-306947
980 66. Feng, X. & McDonald, J. M. Disorders of bone remodeling. *Annu Rev Pathol* **6**, 121-145
981 (2011). https://doi.org:10.1146/annurev-pathol-011110-130203
982 67. Sims, N. A. & Martin, T. J. Osteoclasts Provide Coupling Signals to Osteoblast Lineage
983 Cells Through Multiple Mechanisms. *Annu Rev Physiol* **82**, 507-529 (2020).
984 https://doi.org:10.1146/annurev-physiol-021119-034425
985 68. Signer, R. A. & Morrison, S. J. Mechanisms that regulate stem cell aging and life span. *Cell*
986 *Stem Cell* **12**, 152-165 (2013). https://doi.org:10.1016/j.stem.2013.01.001

987 69. Seike, M., Omatsu, Y., Watanabe, H., Kondoh, G. & Nagasawa, T. Stem cell niche-specific
988 Ebf3 maintains the bone marrow cavity. *Genes Dev* **32**, 359-372 (2018).
989 https://doi.org:10.1101/gad.311068.117
990 70. Mizoguchi, T. *et al.* Osterix marks distinct waves of primitive and definitive stromal
991 progenitors during bone marrow development. *Dev Cell* **29**, 340-349 (2014).
992 https://doi.org:10.1016/j.devcel.2014.03.013
993 71. Maes, C. *et al.* Osteoblast precursors, but not mature osteoblasts, move into developing and
994 fractured bones along with invading blood vessels. *Dev Cell* **19**, 329-344 (2010).
995 https://doi.org:10.1016/j.devcel.2010.07.010
996 72. Shen, B. *et al.* A mechanosensitive peri-arteriolar niche for osteogenesis and lymphopoiesis.
997 *Nature* **591**, 438-444 (2021). https://doi.org:10.1038/s41586-021-03298-5
998 73. Devignes, C. S. *et al.* HIF signaling in osteoblast-lineage cells promotes systemic breast
999 cancer growth and metastasis in mice. *Proc Natl Acad Sci U S A* **115**, E992-E1001
1000 (2018). https://doi.org:10.1073/pnas.1718009115
1001 74. Ambrosi, T. H. *et al.* Distinct skeletal stem cell types orchestrate long bone skeletogenesis.
1002 *Elife* **10** (2021). https://doi.org:10.7554/eLife.66063
1003 75. Cenci, S., Weitzmann, M. N., Gentile, M. A., Aisa, M. C. & Pacifici, R. M-CSF
1004 neutralization and egr-1 deficiency prevent ovariectomy-induced bone loss. *J Clin*
1005 *Invest* **105**, 1279-1287 (2000). https://doi.org:10.1172/JCI8672
1006 76. Cenci, S. *et al.* Estrogen deficiency induces bone loss by enhancing T-cell production of
1007 TNF-alpha. *J Clin Invest* **106**, 1229-1237 (2000). https://doi.org:10.1172/JCI11066
1008 77. Cao, J. J. *et al.* Aging increases stromal/osteoblastic cell-induced osteoclastogenesis and
1009 alters the osteoclast precursor pool in the mouse. *J Bone Miner Res* **20**, 1659-1668
1010 (2005). https://doi.org:10.1359/JBMR.050503

78. Nakashima, T. *et al.* Evidence for osteocyte regulation of bone homeostasis through RANKL expression. *Nat Med* **17**, 1231-1234 (2011). https://doi.org:10.1038/nm.2452

79. Wakkach, A., Rouleau, M. & Blin-Wakkach, C. Osteoimmune Interactions in Inflammatory Bowel Disease: Central Role of Bone Marrow Th17 TNFalpha Cells in Osteoclastogenesis. *Front Immunol* **6**, 640 (2015). https://doi.org:10.3389/fimmu.2015.00640

80. Komori, T. Regulation of osteoblast differentiation by transcription factors. *J Cell Biochem* **99**, 1233-1239 (2006). https://doi.org:10.1002/jcb.20958

81. Aurrand-Lions, M. & Mancini, S. J. C. Murine Bone Marrow Niches from Hematopoietic Stem Cells to B Cells. *Int J Mol Sci* **19** (2018). https://doi.org:10.3390/ijms19082353

82. Bonaud, A., Lemos, J. P., Espeli, M. & Balabanian, K. Hematopoietic Multipotent Progenitors and Plasma Cells: Neighbors or Roommates in the Mouse Bone Marrow Ecosystem? *Front Immunol* **12**, 658535 (2021). https://doi.org:10.3389/fimmu.2021.658535

83. Kusumbe, A. P., Ramasamy, S. K. & Adams, R. H. Coupling of angiogenesis and osteogenesis by a specific vessel subtype in bone. *Nature* **507**, 323-328 (2014). https://doi.org:10.1038/nature13145

84. Xu, J. *et al.* Comparison of skeletal and soft tissue pericytes identifies CXCR4(+) bone forming mural cells in human tissues. *Bone Res* **8**, 22 (2020). https://doi.org:10.1038/s41413-020-0097-0

85. Bisio, V., Espeli, M., Balabanian, K. & Anginot, A. Culture, Expansion and Differentiation of Human Bone Marrow Stromal Cells. *Methods Mol Biol* **2308**, 3-20 (2021). https://doi.org:10.1007/978-1-0716-1425-9_1

86. Ibanez, L. *et al.* Inflammatory Osteoclasts Prime TNFalpha-Producing CD4(+) T Cells and Express CX3 CR1. *J Bone Miner Res* **31**, 1899-1908 (2016). https://doi.org:10.1002/jbmr.2868

87. Schindelin, J. *et al.* Fiji: an open-source platform for biological-image analysis. *Nature methods* **9**, 676-682 (2012). https://doi.org:10.1038/nmeth.2019

88. Kaji, H., Sugimoto, T., Kanatani, M., Nishiyama, K. & Chihara, K. Dexamethasone stimulates osteoclast-like cell formation by directly acting on hemopoietic blast cells and enhances osteoclast-like cell formation stimulated by parathyroid hormone and prostaglandin E2. *J Bone Miner Res* **12**, 734-741 (1997). https://doi.org:10.1359/jbmr.1997.12.5.734

89. Marino, S., Logan, J. G., Mellis, D. & Capulli, M. Generation and culture of osteoclasts. *Bonekey Rep* **3**, 570 (2014). https://doi.org:10.1038/bonekey.2014.65

90. Dobin, A. *et al.* STAR: ultrafast universal RNA-seq aligner. *Bioinformatics* **29**, 15-21 (2013). https://doi.org:10.1093/bioinformatics/bts635

91. Anders, S., Pyl, P. T. & Huber, W. HTSeq--a Python framework to work with high-throughput sequencing data. *Bioinformatics* **31**, 166-169 (2015). https://doi.org:10.1093/bioinformatics/btu638

ACKNOWLEDGMENTS

We thank ML. Aknin (IPSIT, Facility PLAIMMO, Orsay), F. Mercier-Nomé (IPSIT, Facility PHIC, Orsay), Drs. V. Parietti-Montcuquet, C. Doliger, S. Duchez and N. Setterblad (Animal and Flow Cytometry Core Facilities, Institut de Recherche Saint-Louis, Paris), V. Nicolas (IPSIT, Facility MIPSIT, Orsay), D. Courilleau (IPSIT, Facility CIBLOT, Orsay) and C. Cordier and J. Megret (Plateau technique de cytométrie, SFR Necker, Paris) for their technical assistance. We thank the Montpellier Preclinical Platform of the Research Infrastructure ECELLFRANCE for the microCT analyses as well as the Plateforme d'Irradiation (IRSN, Fontenay-Aux-Roses, France) for their technical assistance. The study was supported by the LabEx LERMIT supported by ANR grant ANR-10-LABX-33 under the Program "Investissements d'Avenir" ANR-11-IDEX-0003-01, an ANR PRC grant (ANR-17-CE14-0019) to M.A-L., C.B-W. and coordinated by K.B. and by the Association Saint Louis pour la Recherche sur les Leucémies to KB. J.N. was a PhD fellow from the DIM Cancéropôle and the FRM. Z.A-N. was a fellowship recipient from the French Ministry and from the FRM (FDT202204015088). V.R. was supported by the FRM, La Ligue Contre le Cancer and la Société Française d'Hématologie. A.Bon. was supported by an ANR @RAction grant (ANR-14-ACHN-0008) and by a JCJC ANR grant (ANR-19-CE15-0019-01) to ME. A.Bou. was supported by the ANR grant 17-CE14-0019. J.L. was recipient from the People Program (Marie Curie Actions) of the European Union's Seventh Framework Program (FP7/2007-2013) under REA grant agreement n. PCOFUND-GA-2013-609102, through the PRESTIGE Program coordinated by Campus France, and from an ANR grant (ANR-17-CE14-0019). V.B., N.D. and K.B. were supported by the INCa agency under the program PRT-K 2017. J.K. was supported by European Union's Horizon 2020 MSCA, Program under grant agreement 641833 (ONCORNET). D.H.M and P.M.M. were supported by the Division of Intramural Research of the National Institute of Allergy and Infectious Diseases, National Institutes of Health.

Graphical abstract and mouse icons were created using the Biorender software (Biorender.com).

AUTHOR CONTRIBUTIONS

A.A., J.N. and Z.A-N. designed and performed experiments, analyzed data and contributed to manuscript writing; V.R., A.Bon., M.K., A.Bou., J.L., V.B., J.K., L.S., A.P. and A.C. performed experiments and analyzed data; S.P., N.D., M.A-L., S.J.C.M., G.L., F.G., C.B-W. and M.C-S. performed experiments, contributed to data analyses and reviewed the manuscript; D.H.M. and P.M.M provided WS samples and clinical data and reviewed the manuscript; M.E. and M.R. helped with the study design, performed experiments, contributed to data analyses and reviewed the manuscript; K.B. conceived, designed and supervised the study, contributed to data analyses, found funding for the study, and wrote the manuscript.

COMPETING INTERESTS

The authors declare no competing interests.

TABLES

	Gender	Chronic treatment	Lumbar spine	Femoral neck
P1	Female	No	*-3.1* [5]	0
P2	Female	No	*-1.1*	*-1.8*
P3[1]	Male	Yes [2]	-1.8	*-2.3*
P4	Female	Yes [3]	*-2.7*	*-1.3*
P5[1]	Male	Yes [4]	-1.8	*-2.2*

Table 1: Abnormal bone mineral density values in WS patients. Characteristics of each patient with low BMD value are shown. Four patients carry the *CXCR4*^{R334X} mutation and one displays the *CXCR4*^{S338X} mutation. There were 3 women and 2 men with an average age of 33.2 years (range 13-52). T-scores for lumbar spine (L1-L4) and femoral neck have been evaluated. According to World Health Organization (WHO) criteria, values classify patients as osteopenic with a T-score between -1.0 and -2.5 or osteoporotic with a T-score at or below -2.5.

[1]For patients 3 and 5, because of their young age, Z-scores are given with a value at or below -2.0 considered as abnormal; [2]G-CSF since age of 2; [3]G-CSF several years at the time of scan; [4]G-CSF for 6 months at the time of scan; [5]Values outside the normal range defined by WHO are italicized.

FIGURE LEGENDS

Figure 1: WS-linked *Cxcr4* mutations are associated with reduced bone mass in mice. (A) The bone mineral density (BMD) of lumbar spine of WT, +/1013 and 1013/1013 mice was measured through Dual-energy x-ray absorptiometry. Results represent means ± SEM with 5 mice per group examined over two independent experiments. Statistics were calculated with the nonparametric Kruskal–Wallis H test ($^{\#\#}$p=0.0042) and the nonparametric Mann–Whitney test, two-sided, +/1013 p=0.0556, 1013/1013 **p=0.0079. **(B-D)** 3D representative images of trabecular and cortical composites (B) and quantitative µCT analyses of trabecular (C) and cortical (D) parameters of femurs from WT and mutant mice. BV = bone volume; TV = trabecular volume; Tb.Nb = trabecular number; Tb.Sp = trabecular separation; Ct.BV = cortical bone volume; Ct.Th = cortical thickness. Data (means ± SEM) are from three independent experiments with n= 15, 15, and 7 mice in total for WT, +/1013 and 1013/1013 groups, respectively. Statistics were calculated with the nonparametric Kruskal–Wallis H test ($^{\#\#\#}$p=0.0007, BV/TV; p=0.0001, Tb.Nb; p<0.0001, Tb.Sp; Ct.BV, $^{\#\#}$p=0.0072; $^{\#}$p=0.0241) and the unpaired two-tailed Student's t test (+/1013 vs WT **p=0.0556, 1013/1013 vs WT ***p=0.0005, +/1013 vs 1013/1013 §p=0.032 for BV/TV; ***p=0.0005, ***p<0.0001, §§p=0.008 for Tb.Nb; ***p=0.0038, ***p<0.0001, §§§ p<0.0001 for Tb.Sp; **p=0.0072, **p=0.0078 for Ct.BV; *p=0.0147, *p=0.02 for Ct.Th). **(E)** BM sections were stained with toluidine blue. Larger images show 2X inserts in trabecular areas. Bars: 200 µm. Images are representative of at least three independent determinations. **(F)** BM sections were immunostained for osteopontin (Opn) in association with DAPI. Trabeculae are indicated by white arrows. Bars: 250 µm. Images are representative of five independent determinations. **(G and H)** BM sections were stained for chondrocyte (alcian blue, G) or adipocyte (perilipin, H) markers. Bars: 500 (G) or 20 (H) µm. Images are representative of at least six independent determinations. **(I)** Cartilaginous growth plates were evaluated based on overall growth plate

thickness measured on µCT scans. Data (means ± SEM) are from 2 independent experiments with n= 7, 8, and 7 mice in total for WT, +/1013 and 1013/1013 groups, respectively. **(J)** Adipocyte counts were evaluated on perilipin-stained BM sections. Six fields of 3 mm^2 were analyzed per section. Results (means ± SEM) are from 4 independent experiments with 13 mice in total per group. **(K)** Size (left) and weight (right) of WT and mutant mice. Results (means ± SEM) are from five independent experiments with n= 6, 9, and 10 mice in total for WT, +/1013 and 1013/1013 groups, respectively. Mice were littermates, females and age-matched (8-12 wk-old) in A-J and at 8 weeks of age in K. Source data are provided as a Source Data file.

Figure 2: Reduction of skeletal stromal cells in *Cxcr4*^{1013}-bearing mice. (A) Representative dot-plots showing the flow cytometric gating strategies used to sort stroma cells ($CD45^-$ $TER119^-$), differentiated osteoblast progenitor cells (OPCs, $CD45^-TER119^-CD31^-Sca\text{-}1^-$ $CD51^+PDGFR\alpha^{+/-}$) and SSCs ($CD45^-TER119^-CD31^-Sca\text{-}1^+CD51^+PDGFR\alpha^+$) in the mouse bone fraction. **(B)** Absolute numbers of the indicated stroma cell subsets from bone fractions were determined by flow cytometry. Data (means ± SEM) are from at least six independent experiments with n= 31, 31, and 17 mice in total for WT, +/1013 and 1013/1013 groups, respectively. Statistics were calculated with the nonparametric Kruskal–Wallis H test ($^{###}p<0.0001$, OPC) and the unpaired two-tailed Student's t test (1013/1013 vs WT $*p=0.0206$ for SSC; +/1013 vs WT $**p=0.0031$, 1013/1013 vs WT $***p<0.0001$, +/1013 vs 1013/1013 $^{§}p=0.0217$ for OPC). **(C)** Schematic diagram for the generation of CD45.1→CD45.2 short (3 wks)- or long (16 wks)-term BM chimeras. **(D)** Proportions of WT donor $CD45.1^+$ LSK SLAM and leukocytes (Leuko.) recovered from the BM and blood of BM chimeras in $CD45.2^+$ WT or mutant recipients 16 weeks after transplantation. **(E)** Absolute numbers of SSCs and OPCs determined by flow cytometry in bone fractions of BM chimeras in $CD45.2^+$ recipients. Data (means ± SEM) in D and E are from three independent experiments with n= 10 (D) or 11 (E),

9, and 5 mice in total for WT, +/1013 and 1013/1013 recipient groups, respectively. Statistics were calculated with the nonparametric Kruskal–Wallis H test ($^{\#\#}$p=0.0064) and the nonparametric Mann–Whitney test, two-sided (+/1013 vs WT **p=0.0042, 1013/1013 vs WT *p=0.0126, for SSC; +/1013 vs WT **p=0.0031, 1013/1013 vs WT *p=0.0398, for OPC). **(F)** Sixteen weeks after transplantation, BM sections from WT or mutant CD45.2$^+$ recipient mice were immuno-stained for Opn in association with DAPI (bars: 250 μm). Trabeculae are indicated by white arrows. Images are representative of at least three independent determinations. **(G)** Left: Proportions of WT donor CD45.1$^+$ LSK SLAM and leukocytes recovered from the BM and blood of BM chimeras in CD45.2$^+$ WT or mutant recipients 3 weeks after transplantation. Right: Absolute numbers of SSCs and OPCs. Data (means ± SEM) are from three independent experiments with n= 9, 9, and 5 mice in total for WT, +/1013 and 1013/1013 recipient groups, respectively, except for blood chimerism analysis (5 mice per group). Statistics were calculated with the nonparametric Kruskal–Wallis H test ($^{\#}$p=0.0327) and the nonparametric Mann–Whitney test, two-sided (1013/1013 vs WT *p=0.019, +/1013 vs 1013/1013 §p=0.019 for SSC; 1013/1013 vs WT *p=0.017 for OPC). **(H and I)** 3D representative images of trabecular composites (H) and μCT analyses of trabecular parameters (I) of femurs from WT BM-chimeric CD45.2$^+$ WT or mutant recipients 4 months after transplantation. Data (means ± SEM) are from three independent experiments with n= 8, 5, and 5 mice in total for WT, +/1013 and 1013/1013 recipient groups, respectively. Statistics were calculated with the unpaired two-tailed Student's t test (+/1013 vs WT *p=0.033, 1013/1013 vs WT *p=0.024 for BV/TV). WT and mutant mice were littermates, females and age-matched (8-12 wk-old) and adult Boy/J (CD45.1) WT mice at 8 weeks of age were used as BM donors. Source data are provided as a Source Data file.

Figure 3: Cell-extrinsic Cxcr4-mediated regulation of the skeletal landscape. (A) Schematic diagram for the generation of CD45.2→CD45.1 short (3 wks)- or long (16 wks)-term BM chimeras. **(B)** Proportions of WT or mutant donor CD45.2$^+$ LSK SLAM and leukocytes recovered from the BM and blood of BM chimeras in CD45.1$^+$ WT recipients 16 weeks after transplantation. Statistics were calculated with the nonparametric Kruskal–Wallis H test ($^{\#\#\#}$p=0.0008 for SLAM and <0.0001 for Leukocytes) and the unpaired two-tailed Student's t test (+/1013 vs WT **p=0.0036, 1013/1013 vs WT ***p=0.0004, for SLAM; +/1013 vs WT ***p=0.0003, 1013/1013 vs WT ***p<0.0001, for Leukocytes). **(C)** Absolute numbers of SSCs and OPCs in bone fractions of BM chimeras in CD45.1$^+$ recipients. Statistics were calculated with the nonparametric Kruskal–Wallis H test ($^{\#\#}$p=0.009 for SSC and $^{\#\#\#}$p =0.0006) and the unpaired two-tailed Student's t test (1013/1013 vs WT **p=0.0012, +/1013 vs 1013/1013 §§p=0.0076, for SSC; +/1013 vs WT *p=0.029, 1013/1013 vs WT ***p<0.0001, +/1013 vs 1013/1013 §p=0.022, for OPC). Data (means ± SEM) in B and C are from three independent experiments with n= 14 mice in total for WT, +/1013 and 1013/1013 donor groups, respectively, except for blood chimerism analysis (n= 11, 9, and 8 mice in total for WT, +/1013 and 1013/1013 donor groups, respectively). **(D)** Sixteen weeks after transplantation, BM sections from WT CD45.1$^+$ recipient mice were immunostained for Opn in association with DAPI (bars: 250 μm). Trabeculae are indicated by white arrows. Images are representative of at least three independent determinations. **(E)** Left: Proportions of WT or mutant donor CD45.2$^+$ LSK SLAM and leukocytes recovered from the BM and blood of BM chimeras in CD45.1$^+$ WT recipients 3 weeks after transplantation. Right: Absolute numbers of SSCs and OPCs. Data (means ± SEM) are from three independent experiments with n= 6 (SLAM) or 7 (SSC and OPC), 10, and 8 mice in total for WT, +/1013 and 1013/1013 donor groups, respectively, except for blood chimerism analysis (n= 6, 5, and 4 mice in total for WT, +/1013 and 1013/1013 donor groups, respectively). Statistics were calculated with the nonparametric

Kruskal–Wallis H test ($^{\#\#}$p=0.0083 for leukocytes; $^{\#}$p=0.047 for SSC; $^{\#}$p=0.018 for OPC) and the unpaired two-tailed Student's t test (+/1013 vs WT *p=0.021, 1013/1013 vs WT **p=0.0014, for leukocytes; +/1013 vs WT *p=0.046, 1013/1013 vs WT *p=0.029, for SSC; +/1013 vs WT *p=0.034, 1013/1013 vs WT *p=0.01, for OPC). **(F-I)** 3D representative images of trabecular or cortical composites (F and H) and µCT analyses of trabecular or cortical parameters (G and I) of femurs from WT or mutant BM-chimeric CD45.1^{+} WT recipients 4 months after transplantation. Ct.BV = cortical bone volume; Ct.Th = cortical thickness. Data (means ± SEM) in G and I are from two independent experiments with n= 5, 5, and 4 mice in total for WT, +/1013 and 1013/1013 donor groups, respectively. Statistics were calculated with the nonparametric Kruskal–Wallis H test ($^{\#\#}$p=0.0085 for BV/TV; $^{\#\#}$p=0.0069 for Tb.Nb; $^{\#\#\#}$p=0.0001 for Tb.Sp; $^{\#}$p=0.033 for Ct.BV) and the unpaired two-tailed Student's t test (1013/1013 vs WT *p=0.028, +/1013 vs 1013/1013 §p=0.028 for BV/TV; 1013/1013 vs WT *p=0.011, +/1013 vs 1013/1013 §§p=0.0088 for Tb.Nb; +/1013 vs WT *p=0.044, 1013/1013 vs WT ***p<0.0001, +/1013 vs 1013/1013 §§§p=0.0006 for Tb.Sp; 1013/1013 vs WT *p=0.014, +/1013 vs 1013/1013 §p=0.016 for Ct.BV). Donor WT and mutant mice and Boy/J (CD45.1) WT recipient mice were females at 8 weeks of age. Source data are provided as a Source Data file.

Figure 4: Increased bone resorption and reduced bone formation in *Cxcr4^{1013}*-bearing mice. (A) Bone sections were stained for Tartrate Resistant Acid Phosphatase (TRAP) activity (bars: 100 µm). OCLs are visualized as brown-stained TRAP-positive cells attached to bone trabeculae and are indicated by arrows (representative images). **(B)** OCLs were quantified (Oc.S/BS) and (Oc.N/BV). Results represent means ± SEM with 6 mice in total per group over 3 independent experiments. Statistics were calculated with the nonparametric Kruskal–Wallis H test ($^{\#\#\#}$p=0.0006) and the unpaired two-tailed Student's t test (1013/1013 vs WT *p=0.012

for Oc.S/BS; 1013/1013 vs WT *p=0.049 for Oc.N/BV). **(C and D)** Dynamic histomorphometric measures of bone formation. OS/BS = Osteoid number / Bone surface; Obl.S/BS = Osteoblast surface / Bone surface; MS/BS = Mineralized surface / Bone surface; Dbl/BS = Double labelled surface / Bone surface. Data (means ± SEM) are from 3 independent experiments with n= 6, 6, and 5 mice in total for WT, +/1013 and 1013/1013 groups respectively in C, and n= 6, 6, and 5 (for MS/BS) or 6 (for Dbl/BS) mice in total for WT, +/1013 and 1013/1013 groups respectively in D. Statistics were calculated with the nonparametric Kruskal–Wallis H test ($^{\#}$p=0.038) and the unpaired two-tailed Student's t test (1013/1013 vs WT **p=0.0097 for MS/BS; 1013/1013 vs WT *p=0.035 for Dbl/BS). **(E)** The mineral apposition rate (MAR) and bone formation rate (BFR/BS) were determined. Results (means ± SEM) are from 3 independent experiments with n= 6, 6, and 5 (for MAR) or 6 (for BFR/BS) mice in total for WT, +/1013 and 1013/1013 groups respectively. Statistics were calculated with the nonparametric Kruskal–Wallis H test ($^{\#}$p=0.039) and the unpaired two-tailed Student's t test (1013/1013 vs WT *p=0.03, +/1013 vs 1013/1013 §p=0.044). **(F)** Volcano plot analysis of differentially expressed genes obtained by RNA-seq between WT and 1013/1013 OPCs ($p<0.05$; $FC\geq2$) performed on three biological replicates per group with one replicate representing the pool of 3 mice. Data represent analysis of cpm estimates with a log of fold change of more than 1.5 fold and $p< 0.05$ using enhanced Volcano package. **(G and J)** Heatmap representing the relative expression levels of selected genes (osteogenic, G and osteoclastogenic, J) expressed by sorted OPCs. **(H and K)** Normalized counts of osteogenic (H) and osteoclastogenic (K) genes using the DESeq2 method. Data are represented as floating bars (min to max and line equal median) of the three biological replicates per group. For significance testing, DESeq2 uses a Wald test (p values). The Wald test P values from the subset of genes that pass an independent filtering step, are adjusted for multiple testing using the procedure of Benjamini and Hochberg (padj values). **(I)** *In vitro* osteoblastic differentiation of

sorted OPCs evaluated at day 21 post-culture by Alizarin Red S coloration. The images are representative of 3 independent cultures. The quantification (means ± SEM) from three independent experiments with 6 mice in total per group is shown. **(L)** *In vitro* expanded osteogenic cells from bone fractions were cultured with WT CD11b^{+} osteoclast progenitors and stimulated with PGE2/Vitamin D3 (VitD3)/Dexamethasone (Dex) for 8 days. OCLs (TRAP-positive) were identified (left, representative images, bars: 100 µm) and quantified (right). Data (means ± SEM) are from 2 independent experiments with 6 mice in total per group. Statistics were calculated with the nonparametric Kruskal–Wallis H test ($^{\#}$p=0.033) and the unpaired two-tailed Student's t test (+/1013 vs WT *p=0.02 and 1013/1013 vs WT *p=0.014). **(M)** The relative expression levels of osteoclastogenic genes were determined by quantitative PCR in stimulated osteogenic cells (3 mice per group). Each individual sample was run in triplicate and has been standardized for *36B4* expression levels. All mice were littermates, females and age-matched (8-12 wk-old). Source data are provided as a Source Data file.

Figure 5: Impaired osteogenic specification of *Cxcr4^{1013}*-bearing skeletal stromal/stem cells. (A) Ki-67 and DAPI co-staining to analyze by flow cytometry the cell cycle status of SSCs and OPCs from bone fractions. Bar graphs show the percentage of cells (DAPI^{low}Ki-67^{-}) in the quiescent G0 phase. Data (means ± SEM) are from three independent experiments with n= 9, 6, and 6 mice in total for WT, +/1013 and 1013/1013 groups, respectively. Statistics were calculated with the nonparametric Kruskal–Wallis H test ($^{\#}$p=0.029) and the unpaired two-tailed Student's t test (1013/1013 vs WT **p=0.0091). **(B)** Flow-cytometric detection of BrdU staining in SSCs (left). Percentages of BrdU^{+} bone SSCs and OPCs after a 12-day labelling period (right). Data (means ± SEM) are from three independent experiments with six mice in total per group. Statistics were calculated with the nonparametric Kruskal–Wallis H test ($^{\#\#}$p=0.0021) and the unpaired two-tailed Student's t test (+/1013 vs WT *p=0.016, 1013/1013

vs WT **p=0.0011). **(C)** Characterization of some biological processes displaying differential gene expression signatures in sorted SSCs as defined by GSEA and obtained by RNA-seq on 2 (1013/1013) or 3 (WT and +/1013) biological replicates per group with one replicate representing the pool of 3 mice. For significance testing, DESeq2 uses a Wald test (p values). The Wald test P values from the subset of genes that pass an independent filtering step, are adjusted for multiple testing using the procedure of Benjamini and Hochberg (padj values). **(D)** RNA-seq-based heatmap representing the relative expression levels of osteogenic genes. **(E)** Normalized counts of selected osteogenic genes using the DESeq2 method. Data are represented as floating bars (min to max and line equal median) of the 2 or 3 biological replicates per group. For significance testing, DESeq2 uses a Wald test (p values). **(F)** The heatmap shows the relative expression levels (RQ) normalized for *β-actin* expression levels in each sample of selected genes involved in SSC differentiation towards the osteogenic lineage (6 pools of 100 cells *per* condition) by quantitative PCR. **(G)** RQ of the most regulated genes involved in differentiation and cell cycle of SSCs. Data (means ± SEM) are from two independent experiments with 6 mice in total per group. Statistics were calculated with the nonparametric Kruskal–Wallis H test ($^{\#}$p=0.028 for *Runx2*; $^{\#}$p=0.011 for *Ccnd3*) and the unpaired two-tailed Student's t test (1013/1013 vs WT **p=0.0063 for *Runx2*; 1013/1013 vs WT *p=0.048 for *Col1α*; +/1013 vs WT *p=0.022 and 1013/1013 vs WT *p=0.02 for *Ccnd3*). **(H)** RNA-seq-based heatmap representing the relative expression levels of osteoclastogenic genes expressed by sorted SSCs. **(I)** Normalized counts of selected osteoclastogenic genes using the DESeq2 method. Data are represented as floating bars (min to max and line equal median) of the 2 or 3 biological replicates per group. For significance testing, DESeq2 uses a Wald test (p values). **(J)** Relative expression of osteoclastogenic genes in SSCs by quantitative PCR. Each individual sample was run in triplicate and has been standardized for *β-actin* expression levels and presented as relative expression to WT. Data (means ± SEM) are from

two independent experiments with 5 mice in total per group. **(K)** Immunofluorescence showing in red Osterix (Osx)-positive cells and in blue DAPI-stained nuclei in WT and mutant mice femurs (bars: 100 μm). Dashed lines indicate the limit between the cartilage growth plate (above the line) and the bone (below the line). Images are representative of at least 3 independent determinations. **(L)** Quantification of Osx^+ cells per mm^2 below the growth plate. Data (means ± SEM) are from 5, 5, and 3 independent mice in total for WT, +/1013 and 1013/1013 groups respectively. Statistics were calculated with the unpaired two-tailed Student's t test (1013/1013 vs WT *p=0.0101). **(M)** Absolute numbers of the indicated stroma cell subsets from marrow fractions determined by flow cytometry. Data (means ± SEM) are from four independent experiments with n= 9, 10, and 7 mice in total for WT, +/1013 and 1013/1013 groups, respectively. Statistics were calculated with the nonparametric Kruskal–Wallis H test ($^{###}$p=0.0004 for stroma; $^{##}$p=0.0013 for OPC) and the unpaired two-tailed Student's t test (+/1013 vs WT **p=0.0011, 1013/1013 vs WT ***p=0.0002, +/1013 vs 1013/1013 §p=0.033, for stroma; +/1013 vs WT **p=0.0049, 1013/1013 vs WT ***p=0.0003, for OPC). All mice were littermates, females and age-matched (8-12 wk-old). Source data are provided as a Source Data file.

Figure 6: Cxcr4 desensitization intrinsically regulates *in vitro* the osteogenic differentiation of skeletal stromal cells. (A) Number of colonies formed from bone fractions in CFU-F assays. Data (means ± SEM) are from two independent experiments with n= 4, 6, and 4 mice in total for WT, +/1013 and 1013/1013 groups respectively. Statistics were calculated with the nonparametric Kruskal–Wallis H test ($^{##}$p=0.002) and the unpaired two-tailed Student's t test (+/1013 vs WT *p=0.029, 1013/1013 vs WT ***p=0.0008). **(B)** After *in vitro* loading with BrdU (5 days) or CTV (3 days), the percentages of $BrdU^+$ (left) or CTV^{low} (right) cells within WT and mutant bone-derived SSCs were determined by flow cytometry.

Data (means ± SEM) are from 3 independent experiments with 6 mice in total per group. Statistics were calculated with the nonparametric Kruskal–Wallis H test ($^{\#}p=0.0231$ and $^{\#\#}p=0.0047$ for $BrdU^{+}$ and CTV^{low} respectively) and the unpaired two-tailed Student's t test (+/1013 vs WT *p=0.031, 1013/1013 vs WT **p=0.0023 for $BrdU^{+}$; +/1013 vs WT *p=0.015, 1013/1013 vs WT **p=0.0054 for CTV^{low}). **(C)** Bar graphs show the percentages of cultured WT or mutant SSCs in the quiescent G0 phase ($DAPI^{low}Ki\text{-}67^{-}$, left) or with an apoptotic phenotype (Annexin V^{+} $DAPI^{-}$, right) as determined by flow cytometry. Data (means ± SEM) are from three (right panel) or five (left panel) independent SSC cultures per genotype. Statistics were calculated using the unpaired two-tailed Student's t test (+/1013 vs WT *p=0.032, 1013/1013 vs WT *p=0.021). **(D)** Doubling time (left) and absolute numbers (right) of WT and mutant SSCs after 3 days of culture. Data (means ± SEM) are from 8, 6, and 5 independent SSC cultures for WT, +/1013 and 1013/1013 groups respectively. Statistics were calculated using the unpaired two-tailed Student's t test (+/1013 vs WT *p=0.028, 1013/1013 vs WT *p=0.033 for doubling-time; 1013/1013 vs WT *p=0.048 for SSC). **(E)** Alkaline phosphatase (Alp) staining was performed 14 days after initiation of the culture of WT and mutant SSCs in osteogenic medium supplemented every two days with 10 µM AMD3100 or vehicle (PBS) (bars: 100 µm). Quantitative analyses (number of Alp^{+} cells) were performed under an inverted microscope. Data (means ± SEM) are from 6 independent cultures per genotype. Statistics were calculated with the nonparametric Kruskal–Wallis H test ($^{\#\#}p=0.0022$) and the unpaired two-tailed Student's t test (+/1013 vs WT **p=0.0075, 1013/1013 vs WT **p=0.0018). **(F)** Alizarin Red staining was performed 21 days after initiation of the culture. Quantitative analyses (means ± SEM) of staining were performed using the osteogenesis assay kit in 12 (vehicle) or 6 (AMD3100) independent cultures per genotype. Statistics were calculated with the nonparametric Kruskal–Wallis H test ($^{\#\#\#}p=0.0002$) and the unpaired two-tailed Student's t test (+/1013 vs WT ***p=0.0005, 1013/1013 vs WT ***p<0.0001). **(G)** Expression levels of

osteogenic genes were determined by quantitative PCR in 6 independent WT and mutant SSC cultures 14 and 21 days after initiation of the osteogenic culture in the presence or absence of AMD3100. Each individual sample was run in triplicate and was standardized for *β-actin* expression levels. Results (means ± SEM) are expressed as relative expression compared to WT samples. Statistics were calculated with the nonparametric Kruskal–Wallis H test ($^{\#}$p=0.038 and 0.0205 for Osx days 14 and 21 respectively; $^{\#}$p=0.024 and 0.015 for Alp days 14 and 21 respectively; $^{\#\#}$p=0.0063 for Opn days 21; $^{\#}$p=0.026 for Ocn days 21) and the unpaired two-tailed Student's t test (1013/1013 vs WT *p=0.0107 and 0.013 for Osx days 14 and 21 respectively; 1013/1013 vs WT *p=0.035 and ***p=0.0001 for Alp days 14 and 21 respectively; +/1013 vs WT *p=0.022 and 1013/1013 vs WT **p=0.0056 for Opn days 21; 1013/1013 vs WT **p=0.0108 for Ocn days 21). All mice were littermates, females and age-matched (8-12 wk-old). Source data are provided as a Source Data file.

Figure 7: Normalization of Cxcr4 signaling rescues the osteogenic properties of *Cxcr4^{1013}*-bearing mouse skeletal cells. (A) Schematic diagram for daily AMD3100 intra-peritoneal (*i.p.*) injection for 21 days in WT and mutant mice. **(B)** Absolute numbers of the indicated stroma cell subsets from bone fractions of WT and mutant mice determined by flow cytometry. Data (means ± SEM) are from 2 independent experiments with 6 PBS injected mice and 11 AMD3100-injected mice in total *per* genotype. Statistics were calculated using the nonparametric Mann–Whitney test, two-sided, 1013/1013 vs WT *p=0.041, 1013/1013 (AMD) vs 1013/1013 (vehicle) $^{\&}$p=0.01 for SSC; 1013/1013 vs WT **p=0.0022, WT (AMD) vs WT (vehicle) $^{\&\&}$p=0.0065, 1013/1013 (AMD) vs 1013/1013 (vehicle) $^{\&\&\&}$p=0.0003 for OPC. **(C)** BM sections from WT and mutant mice treated with vehicle (PBS) or AMD3100 were immunostained for Opn in association with DAPI. Bars: 500µm. Images are representative of 3 independent determinations. **(D)** Bone mineral density (BMD) values of lumbar spine from 6

treated mice in total per group are shown. Statistics were calculated using the nonparametric Mann–Whitney test, two-sided, +/1013 vs WT *p=0.041, 1013/1013 vs WT **p=0.0022, +/1013 (AMD) vs +/1013 (vehicle) $^{\&\&}$p=0.0087, 1013/1013 (AMD) vs 1013/1013 (vehicle) $^{\&}$p=0.026. **(E)** Cortical thickness was measured in sections stained with Toluidine Blue. Both cortices were measured and data are presented as a mean of both cortices from 6 mice in total per group. Statistics were calculated using the nonparametric Mann–Whitney test, two-sided, 1013/1013 vs WT **p=0.026. Data (means ± SEM) displayed in D and E are from 2 independent experiments. All mice were littermates, females and age-matched (8-12 wk-old). Source data are provided as a Source Data file.

Figure 8: BM stromal cells from WS patients displayed *in vitro* impaired osteogenic capacities. (A) Relative expression levels of osteogenic genes were determined by quantitative PCR at day 14 in osteogenic-induced cultures of two WS patients-derived BMSCs and 7 healthy donors-derived BMSCs. Each individual sample was run in triplicate and was standardized for *36B4* expression levels. Results (means ± SEM) are expressed as relative expression compared to healthy samples (set at 1 and representing the mean of the 7 healthy donors) and are from 2 independent experiments. Statistics were calculated using the nonparametric Mann–Whitney test, two-sided, **p=0.0079 for OSX, RUNX2 and OCN; *p=0.0179 for OPN. **(B)** Alizarin Red staining was performed 21 days after initiation of the culture of 1.5 x 10^3 healthy or WS BMSCs in pro-osteogenic medium (left panel). Representative images for healthy (H) and WS donors #1 and #2 are shown. Quantitative analyses of staining (means ± SEM) were performed using the osteogenesis assay kit in 3 independent cultures with 2 WS and 6 healthy donors (right panel). Statistics were calculated using the nonparametric Mann–Whitney test, two-sided, **p=0.0022 for healthy. **(C)** Oil Red O staining was performed 21 days after initiation of cultures of healthy or WS BMSCs in pro-adipogenic differentiation medium. Bars: 200µm. **(D)**

Proposed model: Proper Cxcr4 signaling termination is essential for bone tissue homeostasis. Absence of Cxcr4 desensitization leads to imbalance in bone remodeling with decreased OBL-mediated bone formation and increased OCL-mediated bone resorption, leading to severe trabecular and cortical alterations and a subsequent osteoporotic-like phenotype. Mechanistically, impaired Cxcr4 desensitization disrupts the osteogenic commitment of SSCs, while strikingly increasing their pro-osteoclastogenic capacities. Source data are provided as a Source Data file.

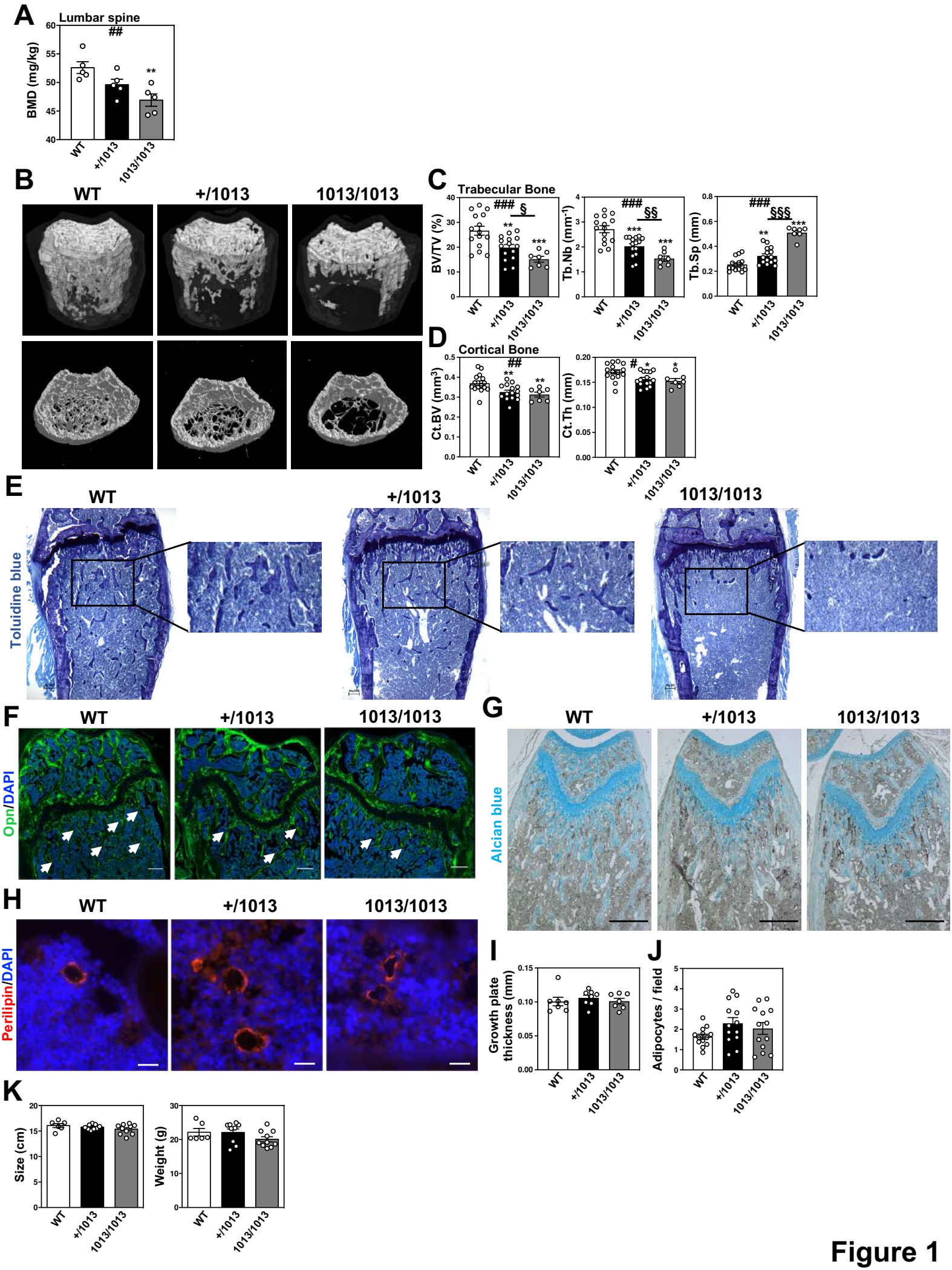
A
Lumbar spine
BMD (mg/kg)
WT
+/1013
1013/1013
B
C
Trabecular Bone
BV/TV (%)
Tb.Nb (mm-1)
Tb.Sp (mm)
D
Cortical Bone
Ct.BV (mm3)
Ct.Th (mm)
E
Toluidine blue
F
Opn/DAPI
G
Alcian blue
H
Perilipin/DAPI
I
Growth plate thickness (mm)
J
Adipocytes / field
K
Size (cm)
Weight (g)

Figure 1

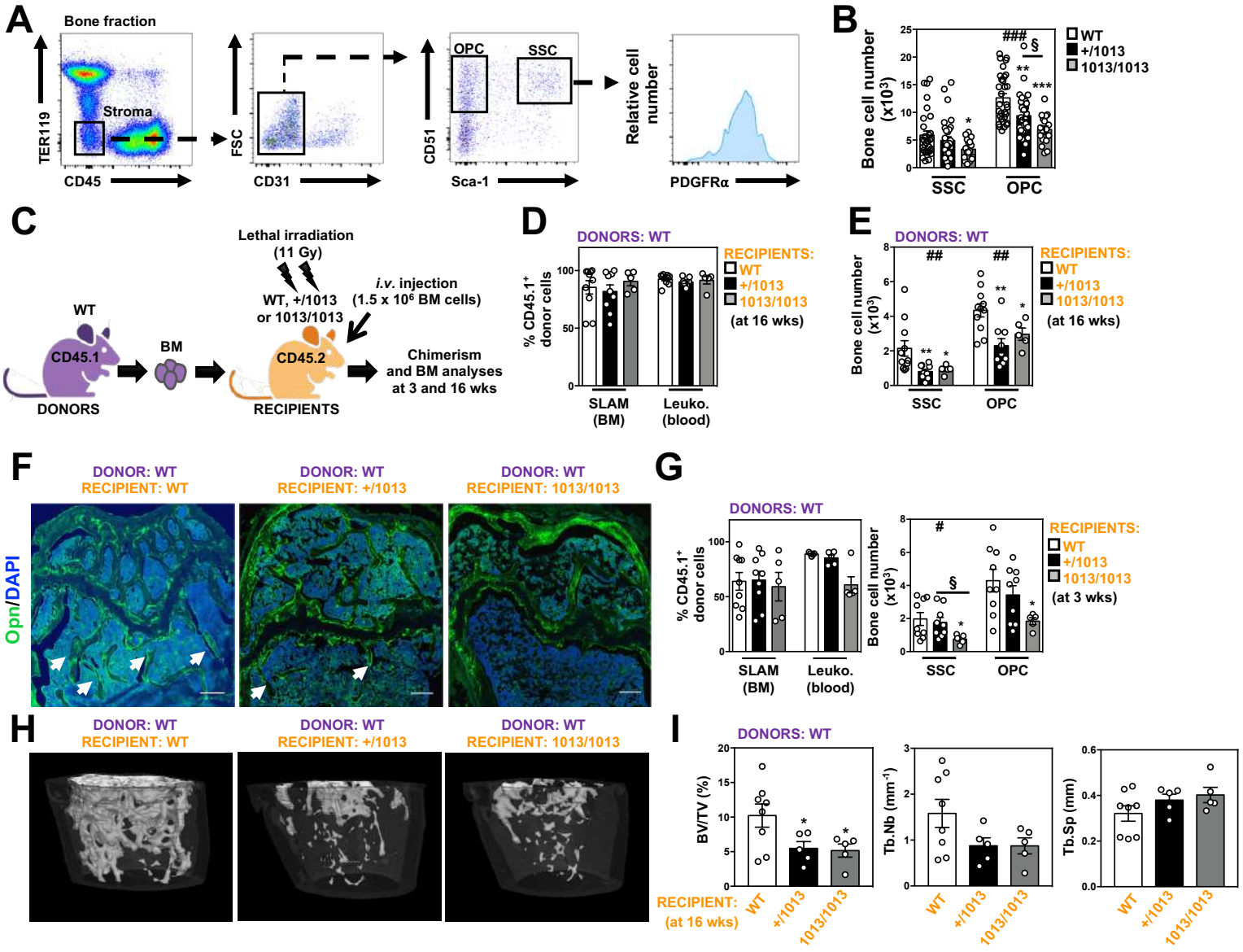
A
Bone fraction
Stroma
TER119
CD45
FSC
CD31
OPC
SSC
CD51
Sca-1
Relative cell number
PDGFRα
B
Bone cell number (x10³)
WT
+/1013
1013/1013
SSC
OPC
C
Lethal irradiation (11 Gy)
WT, +/1013 or 1013/1013
i.v. injection (1.5 x 10⁶ BM cells)
WT
CD45.1
DONORS
BM
CD45.2
RECIPIENTS
Chimerism and BM analyses at 3 and 16 wks
D
DONORS: WT
% CD45.1⁺ donor cells
RECIPIENTS:
WT
+/1013
1013/1013
(at 16 wks)
SLAM (BM)
Leuko. (blood)
E
DONORS: WT
Bone cell number (x10³)
RECIPIENTS:
WT
+/1013
1013/1013
(at 16 wks)
SSC
OPC
F
DONOR: WT
RECIPIENT: WT
DONOR: WT
RECIPIENT: +/1013
DONOR: WT
RECIPIENT: 1013/1013
Opn/DAPI
G
DONORS: WT
% CD45.1⁺ donor cells
Bone cell number (x10³)
RECIPIENTS:
WT
+/1013
1013/1013
(at 3 wks)
SLAM (BM)
Leuko. (blood)
SSC
OPC
H
DONOR: WT
RECIPIENT: WT
DONOR: WT
RECIPIENT: +/1013
DONOR: WT
RECIPIENT: 1013/1013
I
DONORS: WT
BV/TV (%)
Tb.Nb (mm⁻¹)
Tb.Sp (mm)
RECIPIENT: (at 16 wks)
WT
+/1013
1013/1013

Figure 2

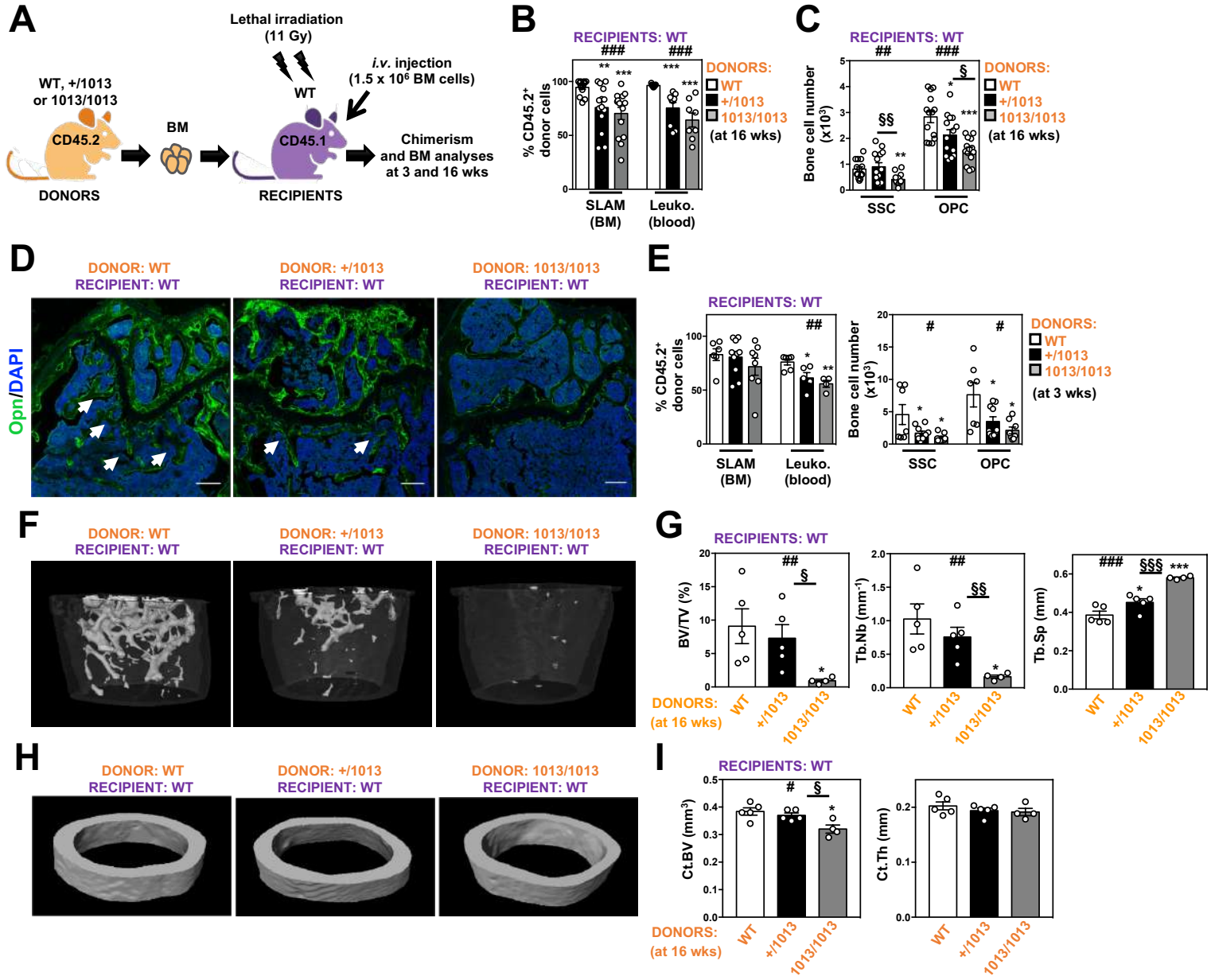
A
Lethal irradiation
(11 Gy)
WT
i.v. injection
(1.5 x 10⁶ BM cells)
WT, +/1013
or 1013/1013
CD45.2
BM
CD45.1
Chimerism
and BM analyses
at 3 and 16 wks
DONORS
RECIPIENTS
B
RECIPIENTS: WT
% CD45.2⁺ donor cells
DONORS:
WT
+/1013
1013/1013
(at 16 wks)
SLAM (BM)
Leuko. (blood)
C
RECIPIENTS: WT
Bone cell number (x10³)
DONORS:
WT
+/1013
1013/1013
(at 16 wks)
SSC
OPC
D
DONOR: WT
RECIPIENT: WT
DONOR: +/1013
RECIPIENT: WT
DONOR: 1013/1013
RECIPIENT: WT
Opn/DAPI
E
RECIPIENTS: WT
% CD45.2⁺ donor cells
Bone cell number (x10³)
DONORS:
WT
+/1013
1013/1013
(at 3 wks)
SLAM (BM)
Leuko. (blood)
SSC
OPC
F
DONOR: WT
RECIPIENT: WT
DONOR: +/1013
RECIPIENT: WT
DONOR: 1013/1013
RECIPIENT: WT
G
RECIPIENTS: WT
BV/TV (%)
Tb.Nb (mm⁻¹)
Tb.Sp (mm)
DONORS:
(at 16 wks)
WT
+/1013
1013/1013
H
DONOR: WT
RECIPIENT: WT
DONOR: +/1013
RECIPIENT: WT
DONOR: 1013/1013
RECIPIENT: WT
I
RECIPIENTS: WT
Ct.BV (mm³)
Ct.Th (mm)
DONORS:
(at 16 wks)
WT
+/1013
1013/1013

Figure 3

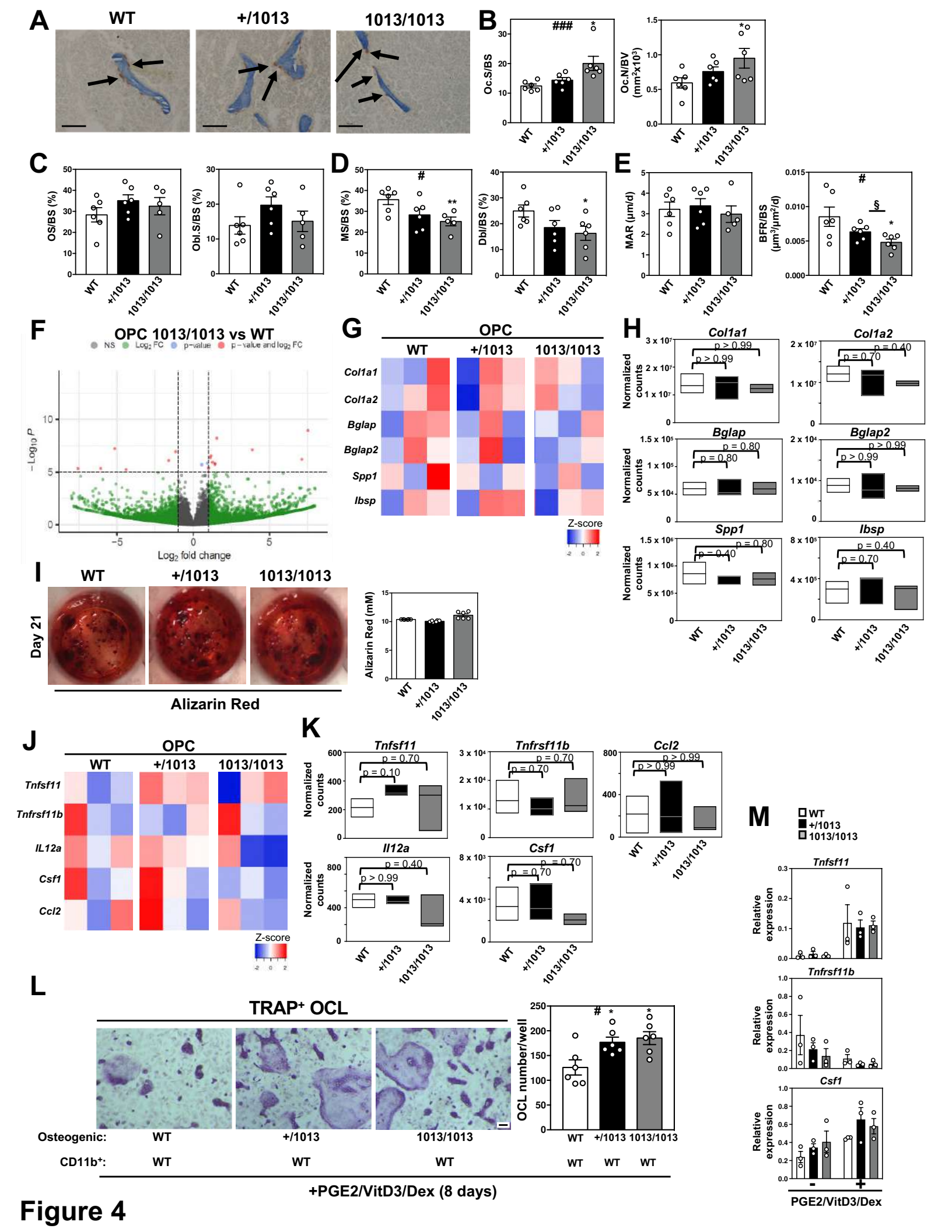
A
WT
+/1013
1013/1013
B
Oc.S/BS
Oc.N/BV (mm²x10³)
C
OS/BS (%)
Obl.S/BS (%)
D
MS/BS (%)
Dbl/BS (%)
E
MAR (µm/d)
BFR/BS (µm³/µm²/d)
F
OPC 1013/1013 vs WT
NS
Log2 FC
p-value
p-value and log2 FC
−Log10 P
Log2 fold change
G
OPC
Col1a1
Col1a2
Bglap
Bglap2
Spp1
Ibsp
Z-score
H
Normalized counts
p = 0.80
p = 0.40
p = 0.70
p > 0.99
I
Day 21
Alizarin Red
Alizarin Red (mM)
J
Il12a
Csf1
Ccl2
K
Tnfsf11
Tnfrsf11b
p = 0.10
M
Relative expression
PGE2/VitD3/Dex
L
TRAP⁺ OCL
OCL number/well
Osteogenic:
CD11b⁺:
+PGE2/VitD3/Dex (8 days)

Figure 4

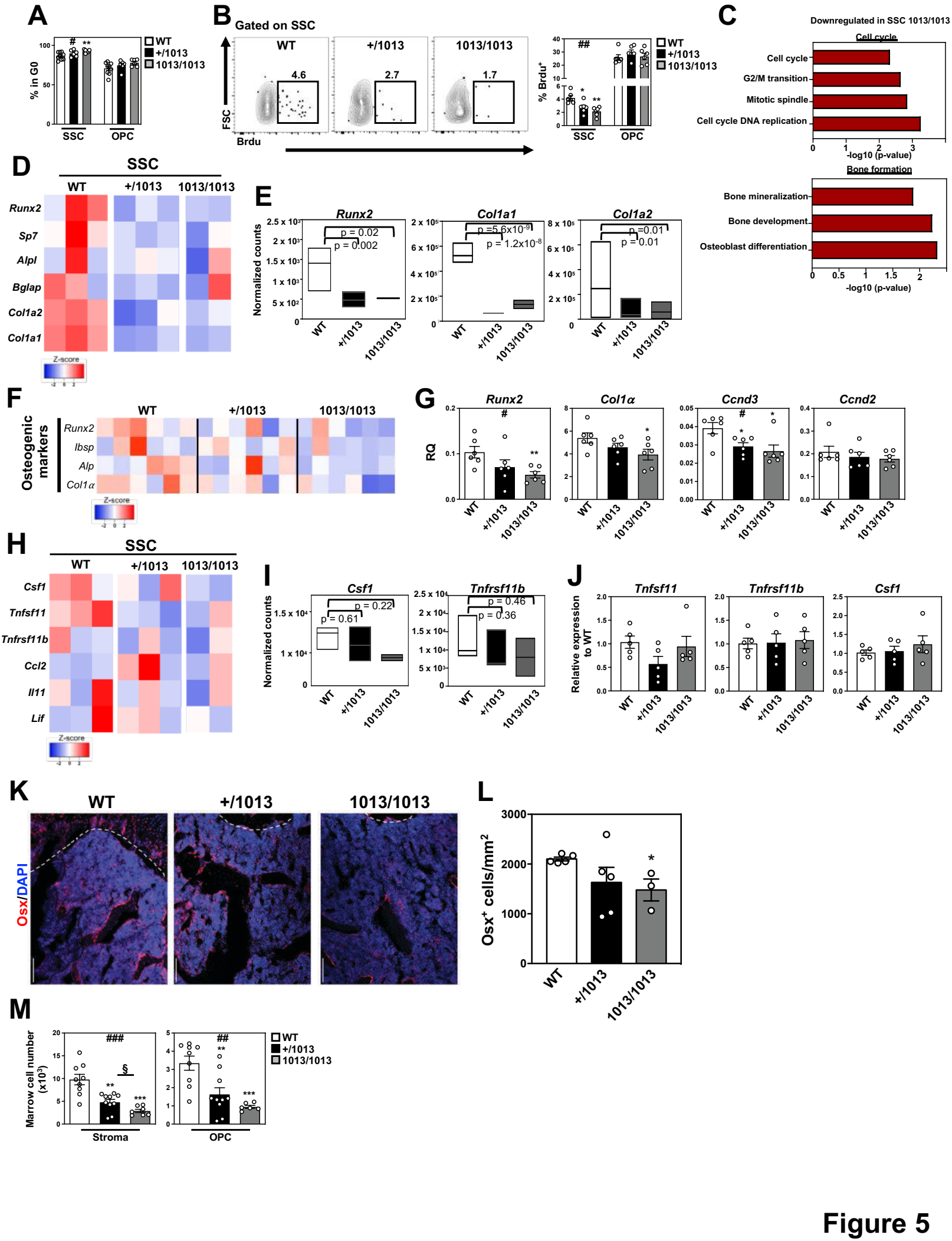
A
% in G0
WT
+/1013
1013/1013
SSC
OPC
B
Gated on SSC
WT
+/1013
1013/1013
4.6
2.7
1.7
FSC
Brdu
% Brdu+
SSC
OPC
C
Downregulated in SSC 1013/1013
Cell cycle
Cell cycle
G2/M transition
Mitotic spindle
Cell cycle DNA replication
-log10 (p-value)
Bone formation
Bone mineralization
Bone development
Osteoblast differentiation
-log10 (p-value)
D
SSC
WT
+/1013
1013/1013
Runx2
Sp7
Alpl
Bglap
Col1a2
Col1a1
Z-score
E
Runx2
Col1a1
Col1a2
Normalized counts
p = 0.02
p = 0.002
p =5.6x10-9
p = 1.2x10-8
p =0.01
p = 0.01
WT
+/1013
1013/1013
F
WT
+/1013
1013/1013
Osteogenic markers
Runx2
Ibsp
Alp
Col1α
Z-score
G
Runx2
Col1α
Ccnd3
Ccnd2
RQ
WT
+/1013
1013/1013
H
SSC
WT
+/1013
1013/1013
Csf1
Tnfsf11
Tnfrsf11b
Ccl2
Il11
Lif
Z-score
I
Csf1
Tnfrsf11b
Normalized counts
p = 0.22
p = 0.61
p = 0.46
p = 0.36
WT
+/1013
1013/1013
J
Tnfsf11
Tnfrsf11b
Csf1
Relative expression to WT
WT
+/1013
1013/1013
K
WT
+/1013
1013/1013
Osx/DAPI
L
Osx+ cells/mm2
WT
+/1013
1013/1013
M
Marrow cell number (x10³)
Stroma
OPC
WT
+/1013
1013/1013

Figure 5

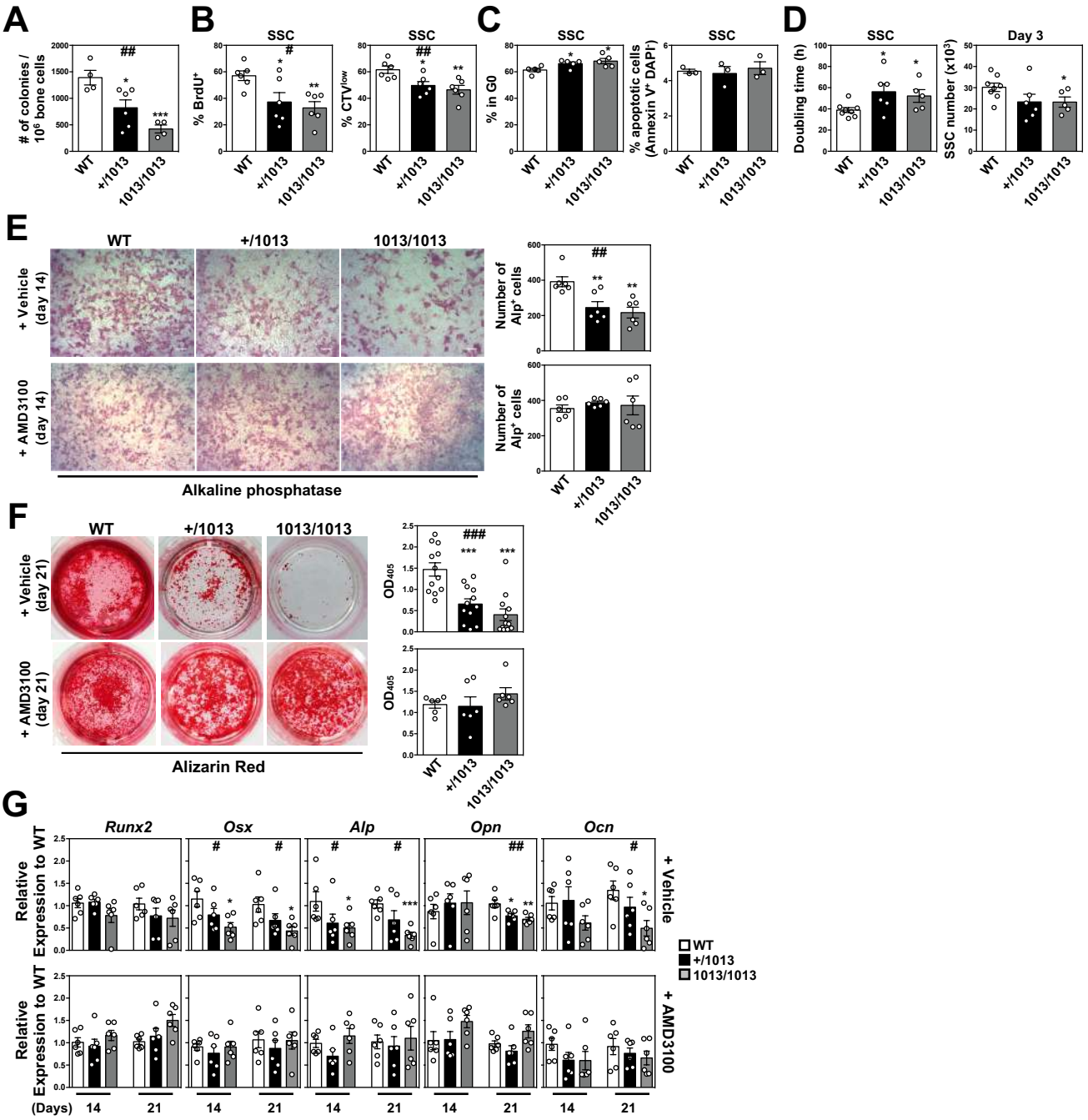
A
B
C
D
E
F
G
WT
+/1013
1013/1013
SSC
Day 3
+ Vehicle (day 14)
+ AMD3100 (day 14)
Alkaline phosphatase
+ Vehicle (day 21)
+ AMD3100 (day 21)
Alizarin Red
Runx2
Osx
Alp
Opn
Ocn
Relative Expression to WT
(Days)
14
21

Figure 6

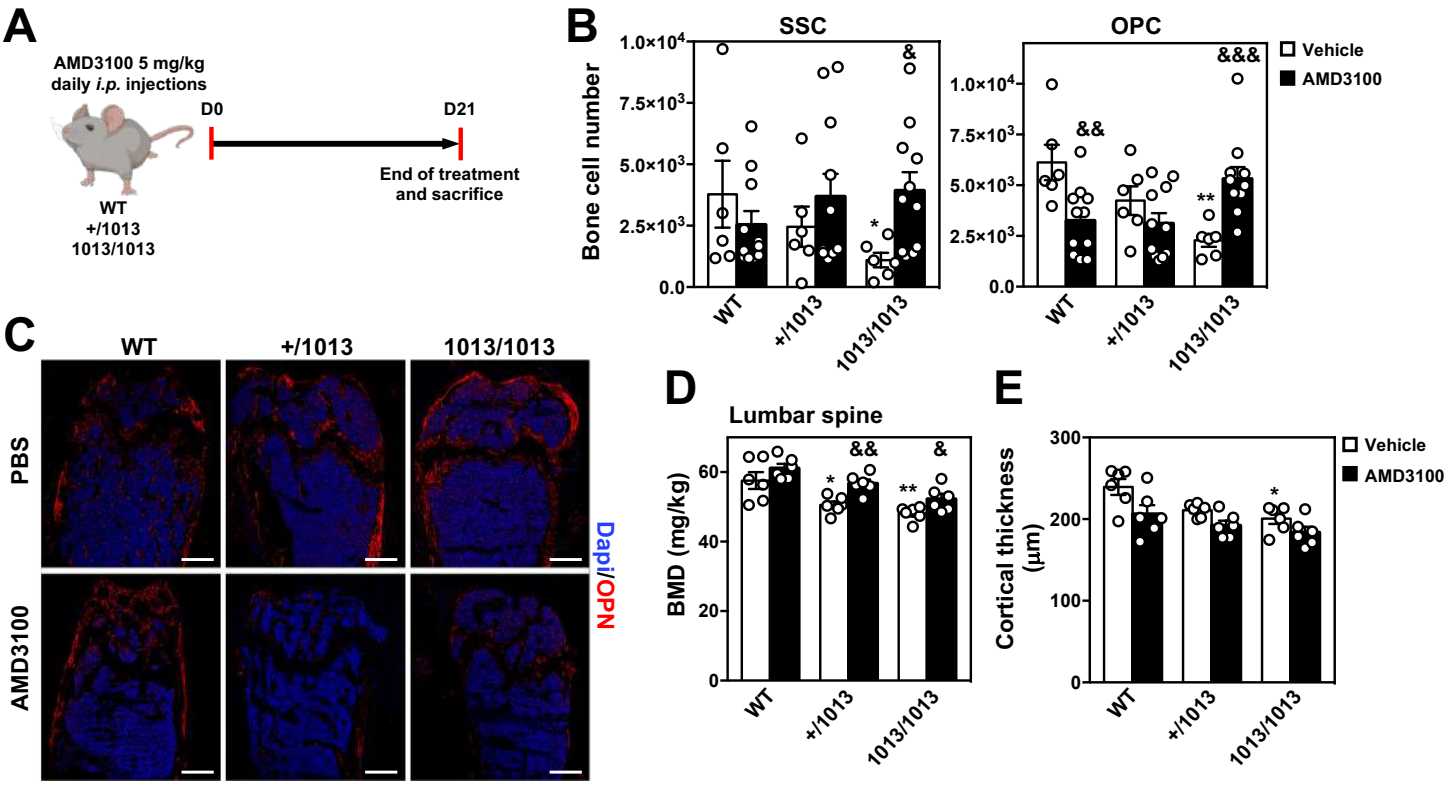
A
AMD3100 5 mg/kg
daily i.p. injections
D0
D21
End of treatment
and sacrifice
WT
+/1013
1013/1013
B
SSC
OPC
Bone cell number
1.0×10^4
7.5×10^3
5.0×10^3
2.5×10^3
0.0
Vehicle
AMD3100
WT
+/1013
1013/1013
C
WT
+/1013
1013/1013
PBS
AMD3100
Dapi/OPN
D
Lumbar spine
BMD (mg/kg)
60
40
20
0
E
Cortical thickness (µm)
300
200
100
0

Figure 7

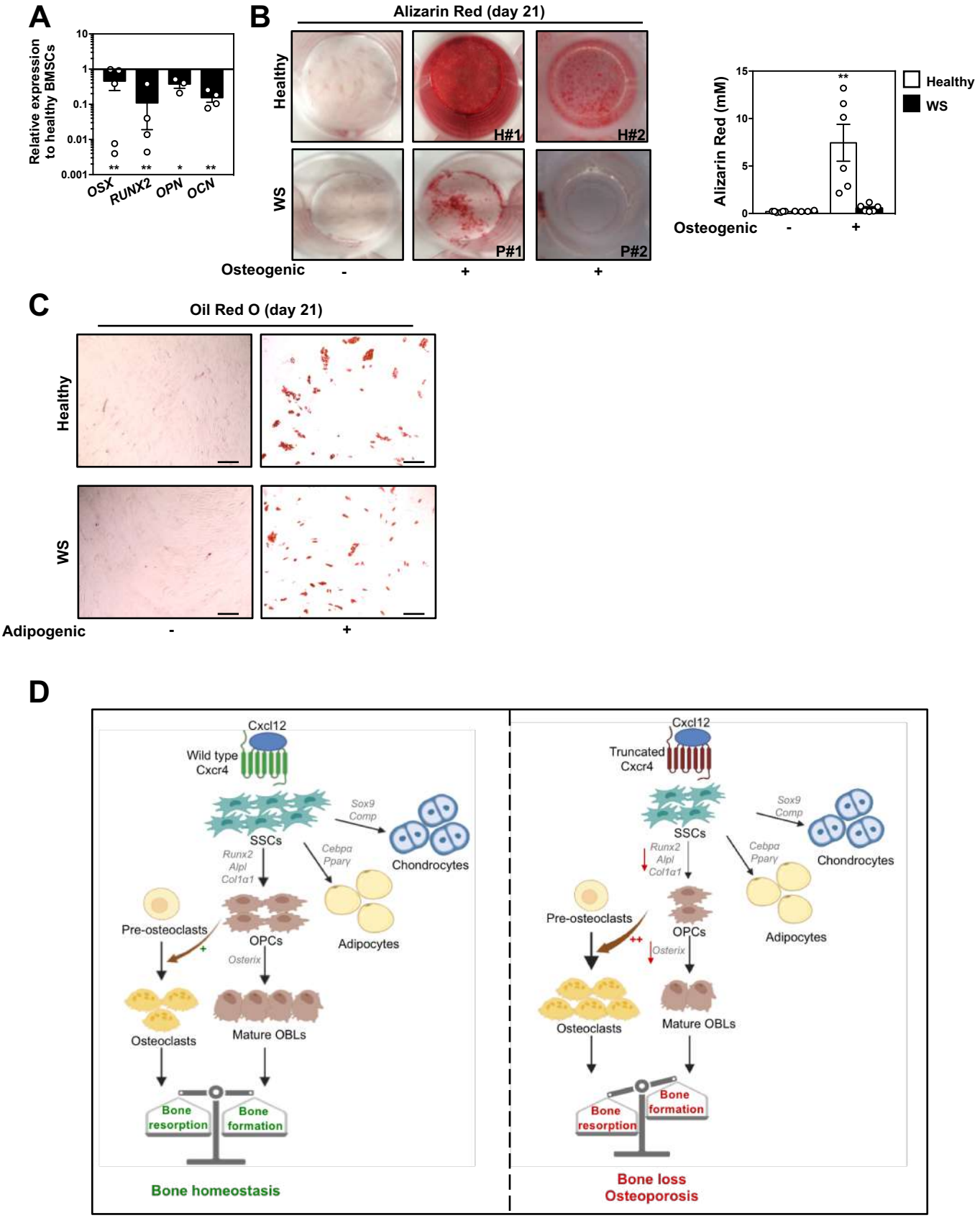
A
Relative expression to healthy BMSCs
10
1
0.1
0.01
0.001
**
**
*
**
OSX
RUNX2
OPN
OCN
B
Alizarin Red (day 21)
Healthy
WS
H#1
H#2
P#1
P#2
Osteogenic - + +
Alizarin Red (mM)
15
10
5
0
**
Healthy
WS
Osteogenic - +
C
Oil Red O (day 21)
Healthy
WS
Adipogenic - +
D
Cxcl12
Wild type Cxcr4
SSCs
Sox9 Comp
Chondrocytes
Runx2 Alpl Col1a1
Cebpa Ppary
Adipocytes
Pre-osteoclasts
OPCs
Osterix
Osteoclasts
Mature OBLs
Bone resorption
Bone formation
Bone homeostasis
Cxcl12
Truncated Cxcr4
SSCs
Sox9 Comp
Chondrocytes
Runx2 Alpl Col1a1
Cebpa Ppary
Adipocytes
Pre-osteoclasts
++
OPCs
Osterix
Osteoclasts
Mature OBLs
Bone resorption
Bone formation
Bone loss
Osteoporosis

Figure 8